ChemRxiv™

doi.org/10.26434/chemrxiv.12091176.v1

Targeted Degradation of Oncogenic KRASG12C by VHL-recruiting PROTACs

Michael J. Bond, Ling Chu, Dhanusha A. Nalawansha, Ke Li, Craig Crews

Submitted date: 07/04/2020 • Posted date: 10/04/2020

Licence: CC BY-NC-ND 4.0

Citation information: Bond, Michael J.; Chu, Ling; Nalawansha, Dhanusha A.; Li, Ke; Crews, Craig (2020): Targeted Degradation of Oncogenic KRASG12C by VHL-recruiting PROTACs. ChemRxiv. Preprint. https://doi.org/10.26434/chemrxiv.12091176.v1

We report the development of LC-2, the first PROTAC capable of degrading endogenous $KRAS^{G12C}$. LC-2 covalently binds $KRAS^{G12C}$ with a MRTX849 warhead and recruits the E3 ligase VHL, inducing rapid and sustained $KRAS^{G12C}$ degradation leading to suppression of MAPK signaling in both homozygous and heterozygous $KRAS^{G12C}$ cell lines. LC-2 demonstrates that PROTAC-mediated degradation is a viable option for attenuating oncogenic KRAS levels and downstream signaling in cancer cells.

File list (3)

4.5.2020.KRAS PROTAC Paper Draft v9.1 CMC.docx (4.16 MiB) view on ChemRxiv • download file

KRAS Supplemental Figures Final v2.pdf (4.69 MiB) view on ChemRxiv • download file

Supporting Information.docx (2.68 MiB) view on ChemRxiv • download file

Title: Targeted Degradation of Oncogenic KRAS^{G12C} by VHL-recruiting PROTACs

Authors: Michael J. Bond[1, †], Ling Chu[2, †], Dhanusha A. Nalawansha[2], Ke Li[2], Craig M. Crews[*,1,2,3]

[1]Department of Pharmacology, Yale University, New Haven, Connecticut 06511, United States

[2]Department of Molecular, Cellular, and Developmental Biology, Yale University, 260 Whitney Avenue, New Haven, Connecticut, 06511, United States

[3]Department of Chemistry, Yale University, New Haven, Connecticut 06511, United States

*Corresponding Author; e-mail:craig.crews@yale.edu

[†]These authors contributed equally to this work

Abstract:

KRAS is mutated in ~20% of human cancers and is one of the most sought-after targets for pharmacological modulation, despite having historically been considered “undruggable.” The discovery of potent covalent inhibitors of the KRAS^{G12C} mutant in recent years has sparked a new wave of interest in small molecules targeting KRAS. While these inhibitors have shown promise in the clinic, we wanted to explore PROTAC-mediated degradation as a complementary strategy to modulate mutant KRAS. Herein, we report the development of LC-2, the first PROTAC capable of degrading endogenous KRAS^{G12C}. LC-2 covalently binds KRAS^{G12C} with a MRTX849 warhead and recruits the E3 ligase VHL, inducing rapid and sustained KRAS^{G12C} degradation leading to suppression of MAPK signaling in both homozygous and heterozygous KRAS^{G12C} cell lines. LC-2 demonstrates that PROTAC-mediated degradation is a viable option for attenuating oncogenic KRAS levels and downstream signaling in cancer cells.

Introduction:

The Kirsten rat sarcoma viral oncogene homolog (*KRAS)* gene is one of the most frequently mutated oncogenes in cancer[1-3]. *KRAS* encodes a small, membrane bound GTPase that relays signals from receptor tyrosine kinases (RTKs), promoting cell proliferation, cell differentiation or cell death[4-5]. In normal cells, KRAS functions as a molecular switch, cycling between an inactive, GDP-bound “off” state and an active, GTP-bound “on” state[4, 6]. This switch is tightly regulated by guanine nucleotide exchange factor (GEF) proteins, which exchange GDP for GTP, and GTPase-activating proteins (GAPs), which enhance the intrinsically slow GTPase activity of KRAS[7-9]. GEF and GAP effector proteins bind at one or both of two shallow binding pockets on KRAS termed switch I (residues 30-38) and switch II (residues 59-76), the conformations of which change dramatically

between GDP- and GTP-bound states[6, 10-11]. Somatic *KRAS* mutations attenuate the GAP-mediated enzymatic activity of the protein, resulting in accumulation of GTP-bound, active KRAS and hyperactivation of downstream signaling, which leads to uncontrolled cell proliferation[1, 5]. Despite its prevalence in cancer and many years of extensive research efforts, mutant KRAS has remained a challenging therapeutic target given the scarcity of traditional druggable pockets on its surface[12].

The *KRAS p.G12C* mutation is highly prevalent in lung adenocarcinoma (LUAD). $KRAS^{G12C}$ mutants make up over 50% of all KRAS mutant LUAD tumors (13% of total LUAD tumors)[1]. Additionally, 3% of colorectal cancers and 1% of all other solid tumors express $KRAS^{G12C}$ [13]. This mutation greatly reduces KRAS's intrinsic GTPase activity, allowing for the accumulation of GTP-bound, active KRAS[14]. Recent advances, initially led by the Shokat group, have identified molecules that covalently and selectively bind the mutated cysteine of $KRAS^{G12C}$ [15-18]. These compounds induce a novel, drug-like pocket within the KRAS switch II region[15]. Optimization of the electrophiles responsible for conjugating the cysteine as well as the molecular interactions within the drug-induced pocket have led to the development of orally bioavailable $KRAS^{G12C}$ inhibitors. ARS-1620/ARS-3248, AMG510, and MRTX849, developed by Wellspring, Amgen, and Mirati Therapeutics respectively, have been shown to potently inhibit $KRAS^{G12C}$ activity *in vitro* and *in vivo*[19-22]. In addition, ARS-3248, AMG510 and MRTX849 have entered phase I clinical trials and have shown promising results[23]. However, despite this success, rapid adaptive resistance and MAPK signaling reactivation after inhibitor treatment have already been reported[24-25]. Thus, the development of complementary therapeutic strategies could help realize the full potential of targeting KRAS mutants for cancer treatment.

PROteolysis TArgeting Chimeras (PROTACs) have emerged as a new and promising modality in drug discovery[26-29]. These bifunctional molecules simultaneously engage a protein of interest (POI) and an E3 ligase, forming a ternary complex, enabling the E3 ligase to ubiquitinate the POI on proximal lysine residues[30-31]. The ubiquitinated POI is subsequently recognized and degraded by the 26S proteasome. A major advantage of target degradation is the elimination of scaffolding roles that are not typically attenuated by traditional small-molecule inhibitors[32-36]. PROTACs incorporating ARS-1620 and the cereblon E3 ligase ligand thalidomide were recently published by the Gray group[37-38]. These molecules engage $KRAS^{G12C}$ and degrade an artificial GFP-$KRAS^{G12C}$ fusion protein, but were unable to degrade endogenous KRAS. Herein, we report the development of the first-in-class endogenous $KRAS^{G12C}$ degrader, **LC-2**, which combines **MRTX849** with a VHL E3 ligase ligand[39]. We observe rapid degradation through a bona fide PROTAC mechanism in both homozygous and heterozygous $KRAS^{G12C}$-expressing cells. Acute and sustained degradation of

KRAS^{G12C} in multiple cancer cell lines renders LC-2 a valuable tool compound to interrogate KRAS biology and represents a significant step towards the development of PROTAC-based candidate therapeutics that function by inducing oncogenic KRAS degradation.

Results:

MRTX849 based VHL-recruiting PROTACs engage and degrade endogenous KRAS^{G12C} in homozygous and heterozygous mutant cell lines.

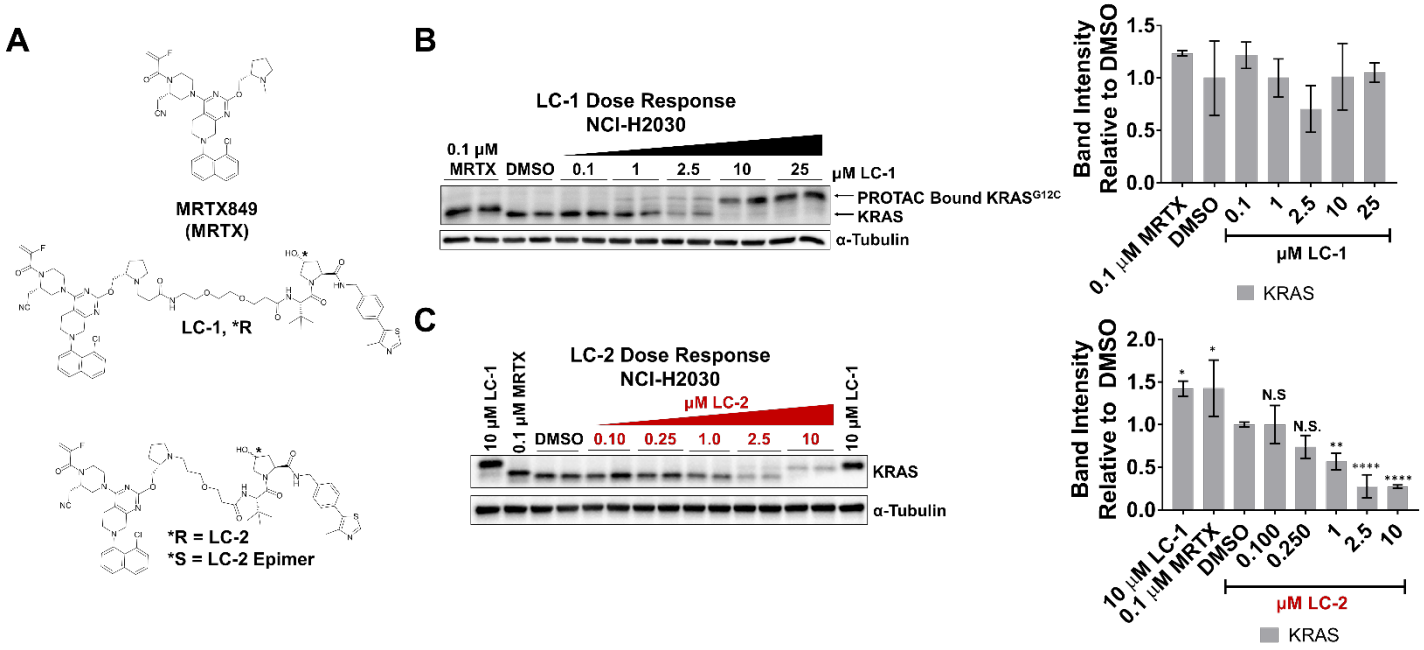

Figure 1: MRTX849-VHL PROTACs engage and degrade endogenous KRASG12C in NCI-H2030 cells: A) Chemical structures of MRTX849, LC-1 (inactive PROTAC), LC-2 (active PROTAC), and LC-2 Epimer. B) LC-1 engages KRASG12C in a dose dependent manner. Quantitation on the right. C) LC-2 degrades KRASG12C in a dose dependent manner. Quantitation on the right. Quantified data represents mean ± SD. Not Significant (N.S.); * $p < 0.05$; ** $p < 0.01$; **** $p < 0.001$

In view of its promising Phase I clinical data and synthetic tractability, we chose **MRTX849** (MRTX; Figure 1A) as a starting point to design KRAS-targeting PROTACs. Docking of **MRTX** into the "switch II" pocket of KRAS^{G12C} reveals the pyrrolidine group to be solvent exposed (PDB: 5V9U; SI Figure 1A)[19]. To avoid introducing another stereocenter at the 2,3 or 4 position of the pyrrolidine and further complicating our synthetic route, we decided to build linkers from the N-methyl moiety of the pyrrolidine. We saw our first evidence of KRAS engagement with **LC-1** (Figure 1A and B). When NCI-H2030 cells were treated with increasing concentrations of **LC-1** for 24 hours we observed a clear band shift at 1, 2.5, 10, and 25 μM, indicating the presence of PROTAC-conjugated KRAS (Figure 1B). However, only a small, non-significant reduction in KRAS levels was observed. Therefore, these data indicate that **LC-1** can engage KRAS^{G12C}, but does not

efficiently degrade the protein. As a result, **LC-1** was subsequently used as a positive control for KRAS engagement during our PROTAC screen.

Cell Line	$KRAS^{G12C}$ Genotype	DC_{50} (μM)	D_{max} (%)	Mirati Sensitivity[21]
NCI-H2030	Homozygous	0.59 ± 0.2	> 75	+
MIA PaCa2	Homozygous	0.32 ± 0.08	> 75	++
SW1573	Homozygous	0.76 ± 0.3	> 85	-
NCI-H23	Heterozygous	0.25 ± 0.08	> 90	+++
NCI-H358	Heterozygous	0.52 ± 0.3	> 40	+++

Table 1. LC-2 induces degradation of endogenous KRASG12C in multiple KRAS mutant cancer cell lines: PROTAC activity in a panel of KRASG12C cancer cell lines. DC50 at which 50% of the maximal degradation (Dmax) is reached.

One major liability of **LC-1** is the presence of a hydrolysable amide within the linker. To address this liability, the linkers of subsequent PROTACs were extended directly from the pyrrolidine ring nitrogen. We screened a small library of PROTACs with linker lengths several atoms shorter and longer than **LC-1**, and from this screen, we identified **LC-2** as the most potent $KRAS^{G12C}$-degrading PROTAC (Figure 1A). **LC-2** induced maximal degradation of endogenous $KRAS^{G12C}$ at concentrations as low as 2.5 μM with a D_{Max} of >75% and a DC_{50} of 0.59 ± 0.2 μM in NCI-H2030 cells (Figure 1C). At 10 μM **LC-2**, a $KRAS^{G12C}$ band running at the same molecular weight as **LC-1**-modified $KRAS^{G12C}$ was observed. The emergence of this undegraded higher molecular weight band suggests the start of a “hook-effect” at high **LC-2** concentrations. The “hook-effect” is a hallmark of PROTACs, whereby at high drug concentrations, the formation of unproductive dimers with target or with E3 ligase outcompete formation of the ternary complex necessary for degradation[40].

MRTX is known to be selective for mutant $KRAS^{G12C}$ over other KRAS mutants [21]. To explore the specificity of **LC-2**, KRAS degradation was examined in HCT 116 cells, which harbor a heterozygous $KRAS^{G13D}$ mutation. No engagement or degradation of $KRAS^{G13D}$ was observed in the presence of **LC-2** up to 10 μM (SI Figure 1B). These data further suggest that **LC-2** selectively engages and degrades mutant $KRAS^{G12C}$ protein.

In addition, we tested **LC-2** in 5 different $KRAS^{G12C}$ cell lines and observed DC_{50} values between 0.25 and 0.76 μM as well as D_{Max} values ranging from >75-90% (Table 1). **LC-2** can degrade

mutant KRAS in both homozygous and heterozygous cell lines with varying sensitivities to **MRTX**[21]. We observed >50% degradation in NCI-H23 cells, which are heterozygous. Theoretically, since these cells carry one wild type and one mutant $KRAS^{G12c}$ allele, one would expect a maximum of 50% degradation if expression were equal, as we see for NCI-H358 cells (SI Figure 2A). However, in siRNA knockdown experiments using $KRAS^{G12C}$ specific siRNA, nearly complete loss of KRAS is observed for NCI-H23 cells, which is consistent with the degradation we observe with **LC-2**[41].Cumulatively, these data show that **MRTX**-based, VHL-recruiting PROTACs can engage and degrade $KRAS^{G12C}$ in multiple cancer cell lines.

LC-2 induced $KRAS^{G12C}$ degradation occurs via a bona fide PROTAC mechanism.

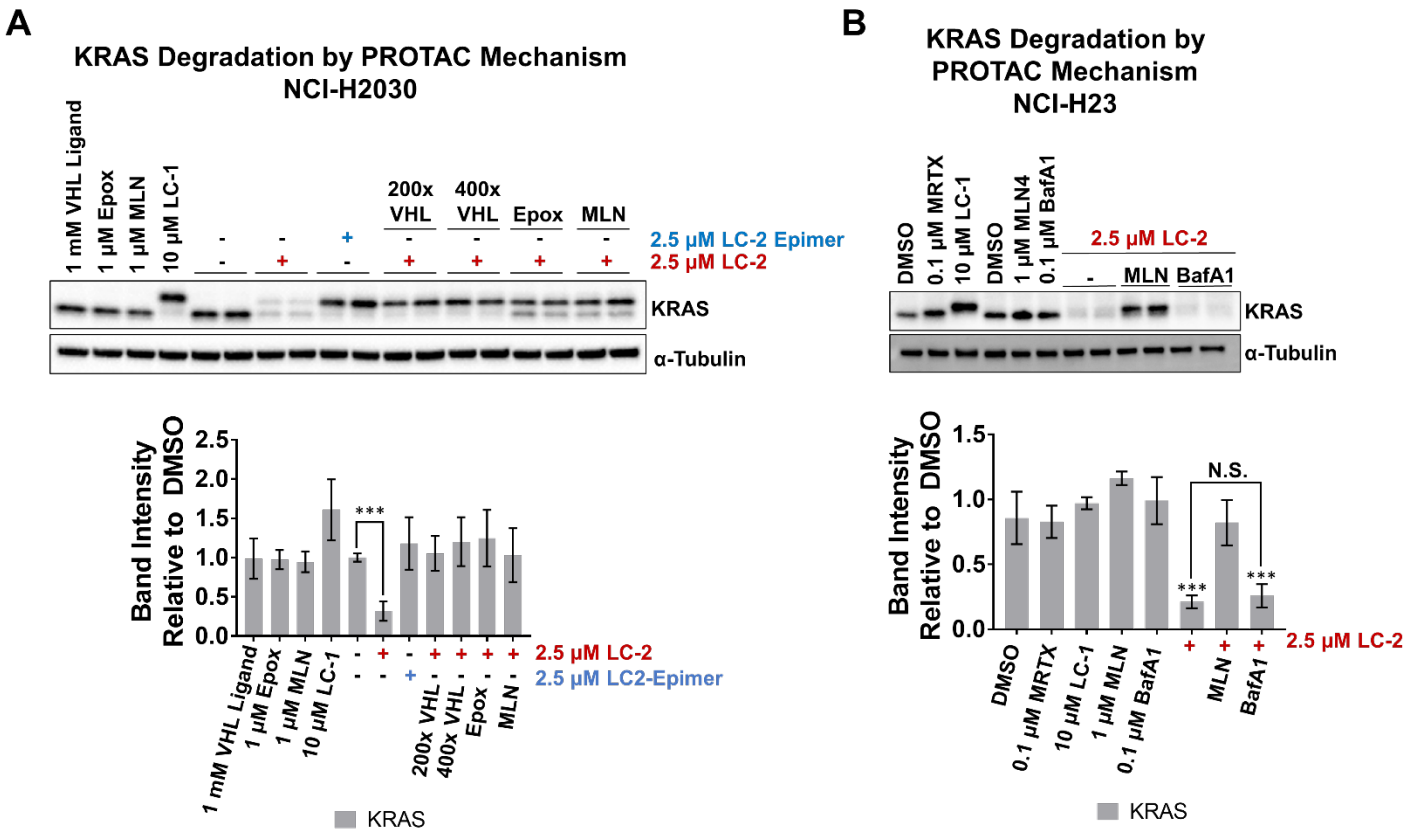

Figure 2: Degradation of endogenous KRASG12C is via a PROTAC mechanism. A) LC-2 Epimer does not induce KRASG12C degradation at 2.5 µM and LC-2 induced degradation is rescued by VHL ligand competition, proteasome inhibition with epoxomicin (Epox), and neddylation inhibition with MLN4924 (MLN), in NCI-H2030 cells. Quantitation is below. B) Inhibition of neddylation, but not inhibition of lysosomal acidification, rescues LC-2 induced KRASG12C degradation in NCI-H23 cells. Quantitation is below. Quantified data represents mean ± SD. Not Significant (N.S.); *** $p < 0.005$

The hydroxy proline moiety of the VHL ligand confers binding to the E3 ligase, while inversion of the absolute stereochemistry of the 4-hydroxy proline moiety abrogates VHL binding[39]. Therefore, we synthesized **LC-2 Epimer** (Figure 1A) as a physicochemically-matched negative control

molecule that is unable to recruit VHL. When NCI-H2030 cells were treated with 2.5 μM **LC-2 Epimer** for 4 hours, only KRAS engagement was observed, whereas 2.5 μM **LC-2** induced significant degradation (~65%; Figure 2A).

PROTACs target proteins for degradation via the proteasome by facilitating their ubiquitination, which is dependent on the formation of a ternary complex[26, 30-31] between the POI, PROTAC and the E3 ligase – in this case, VHL. Since excess VHL ligand inhibits ternary complex formation, we performed competition experiments in NCI-H2030 cells that were pre-treated for 1 hour with molar excess of VHL ligand before being treated with 2.5 μM **LC-2**. Competition of **LC-2** with VHL ligand rescued $KRAS^{G12C}$ levels (Figure 2A) by preventing PROTAC engagement with VHL. However, the higher molecular weight $KRAS^{G12C}$ band observed upon **LC-2** treatment demonstrates that the PROTAC was nevertheless still able to engage $KRAS^{G12C}$.

Neddylation of CUL2, a VHL adaptor protein, is necessary for proper assembly and function of the VHL E3 ligase complex[42]. To further investigate whether **LC-2** induced degradation of $KRAS^{G12C}$ occurs via a bona fide PROTAC mechanism, NCI-H2030 cells were treated with 1 μM of the neddylation inhibitor MLN4924 or 1 μM of the proteasome inhibitor epoxomicin, before being treated with 2.5 μM **LC-2**[43-44]. Both inhibitors rescued $KRAS^{G12C}$ levels suggesting $KRAS^{G12C}$ degradation by **LC-2** is both proteasome- and neddylation-dependent (Figure 2A).

KRAS is tethered to the plasma membrane, and it is possible that monoubiquitination of $KRAS^{G12C}$ could induce endocytosis and degradation of $KRAS^{G12C}$ through the lysosomal pathway[45]. Therefore, we also tested whether bafilomycin A1 (BafA1), an inhibitor of lysosomal acidification, could rescue $KRAS^{G12C}$ degradation[46]. Pre-treatment of NCI-H23 with BafA1 was unable to rescue **LC-2** induced $KRAS^{G12C}$ degradation, whereas neddylation inhibition again rescued KRAS degradation (Figure 2B). Taken together these data show that **LC-2**-induced $KRAS^{G12C}$ degradation is dependent on ternary complex formation with VHL and a functioning ubiquitin proteasome system, but not dependent on the lysosome.

LC-2 induce rapid and sustained $KRAS^{G12C}$ degradation in multiple cancer cell lines

To explore PROTAC-induced $KRAS^{G12C}$ degradation kinetics, time course experiments were performed in NCI-H2030 cells and SW1573 cells using 2.5 μM **LC-2** as the fixed concentration since it induced maximal degradation in all cell lines within 24 hours (Figure 1A and SI Figure 2). To distinguish between rates of target engagement and degradation, **LC-2 Epimer** was used as a negative control to monitor $KRAS^{G12C}$ engagement. Quantitation of engagement was achieved by comparing the intensity of just the **LC-2 Epimer** modified band to the intensity of unbound KRAS in

DMSO treated samples (see *Material and Methods*). For NCI-H2030 cells, KRAS^{G12C} binding was seen as early as 1 hour for both **LC-2** and **LC-2 Epimer** (Figure 3A). Maximal engagement and significant degradation occurred within 4 hours. Maximum degradation was reached by 8 hours in NCI-H2030 cells and persisted up to 24 hours. SW1573 cells showed faster kinetics with near maximal engagement at 1 hour. However, the degradation rate was slower than NCI-H2030 cells as maximal degradation was not observed until 12 hours (Figure 3B)

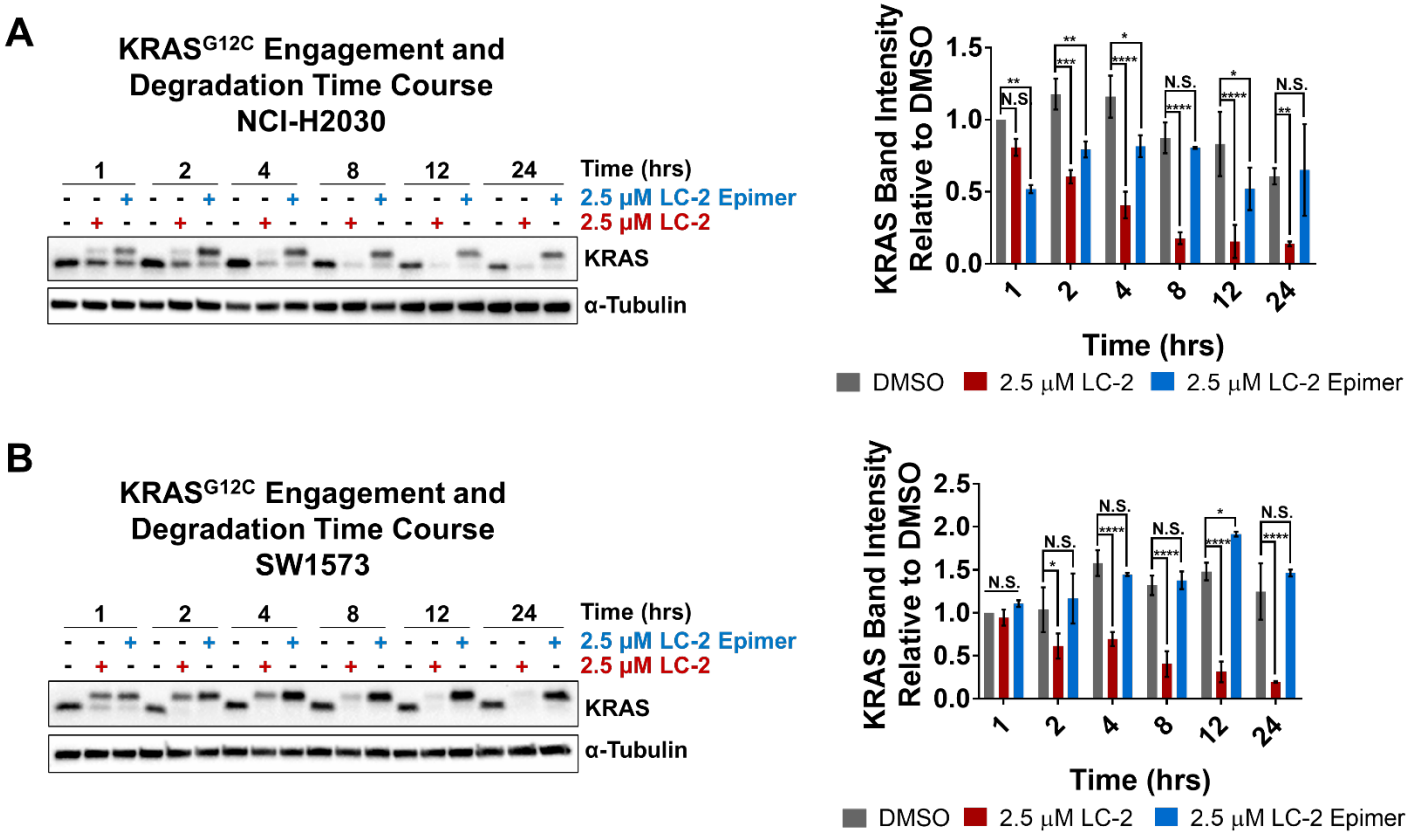

Figure 3: KRASG12C degradation is rapid, with maximal degradation induced as early as 4 hours: A) Time course in NCI-H2030 cells. LC-2 and LC-2 epimer engage within 1 hour with maximal degradation observed by 8 hours and maintained up to 24 hours. Quantitation on the right. B) Time course in SW1573 cells. LC-2 and LC-2 epimer engage KRAS within 1 hour and maximal degradation is observed at 12 hours and maintained up to 24 hours. Quantitation on the right. LC-2 Epimer is a quantification of the higher molecular weight, PROTAC Epimer modified band to monitor engagement of KRASG12C overtime rather than total KRAS levels. Quantified data represents mean ± SD. Not Significant (N.S.); * $p < 0.05$; ** $p < 0.01$; *** $p < 0.005$; **** $p < 0.001$.

During our PROTAC screen, we observed that 0.1 μM of **MRTX** and 10 μM of **LC-1** increased KRAS protein levels (Fig 1C). Although Hallin, *et al.* did not observe increased KRAS^{G12C} protein levels with **MRTX**, our data is consistent with previous observations made with the KRAS^{G12C} inhibitor **ARS1620**[19, 21]. Therefore, we explored how longer treatments with **LC-2** would affect KRAS^{G12C} levels. MIA PaCa-2, NCI-H23, and SW1573 cells were treated with 2.5 μM of **LC-2** for 6,

24, 48, and 72 hours. In all three cell lines maximal KRAS degradation occurred within 24 hours and was sustained up to 72 hours (Figure 4A-B and SI Figure 3). **LC-2 Epimer** fully engaged $KRAS^{G12C}$ in SW1573 cells, but did not decrease protein levels as expected (SI Figure 3). In NCI-H23 cells, $KRAS^{G12C}$ began to rebound at 72 hours. Taken together these data show that **LC-2** is capable of rapid and sustained $KRAS^{G12C}$ degradation in both homozygous and heterozygous cell lines. The ability to overcome increased $KRAS^{G12C}$ expression suggests that degradation could be more beneficial than inhibition for prolonged attenuation of downstream signaling as has been observed previously with BRD4 degraders[47].

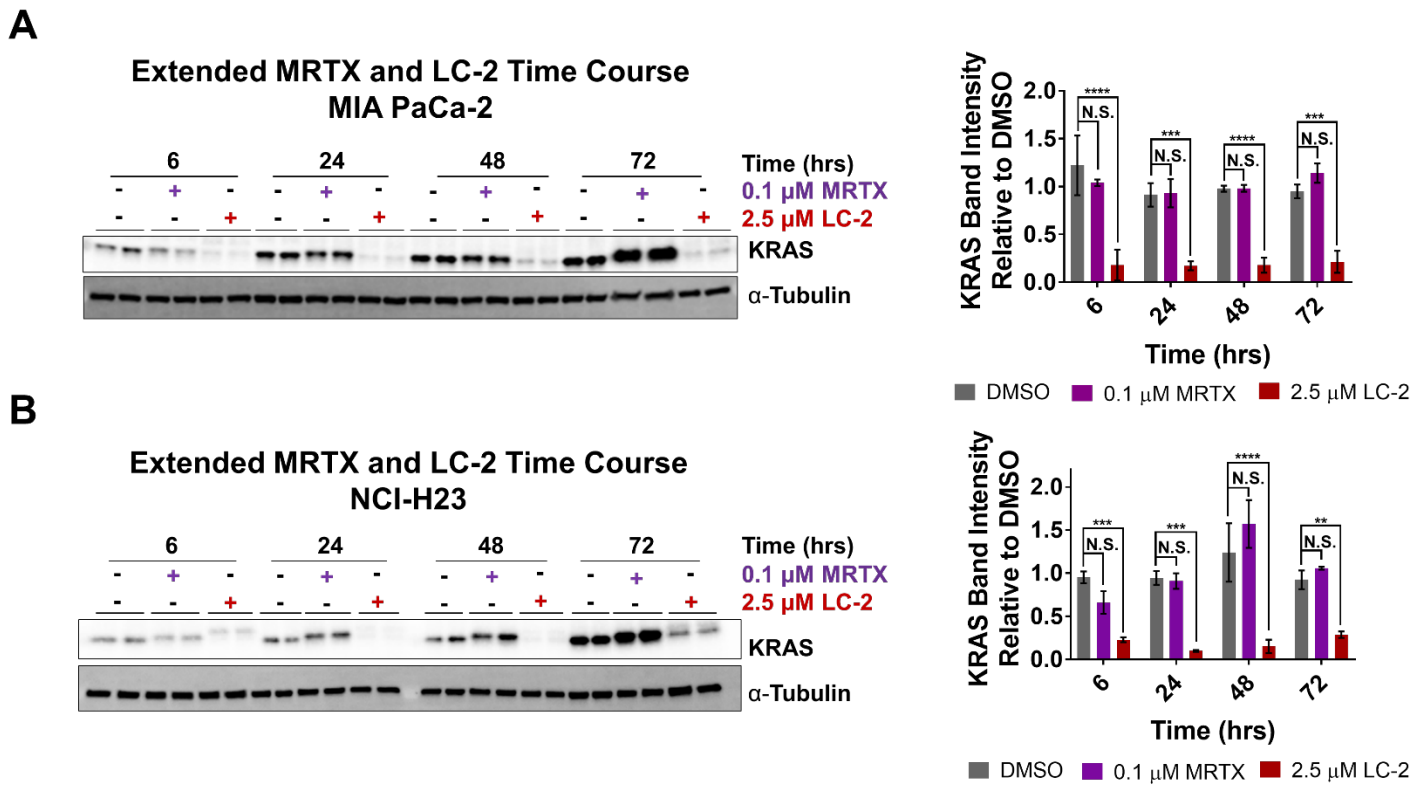

Figure 4: Degradation of endogenous KRASG12C is sustained over 72 hours in multiple cancer cell lines. A) 72 hour time course in MIA PaCa-2 cells. Degradation occurs at 6 hours and is maintained up to 72 hours. Quantitation on the right. B) 72 hour time course in NCI-H23 cells. Degradation occurs within 6 hours, reaches a maximum at 24 hours, and begins to rebound by 72 hours. Quantitation on the right. Quantified data represents mean ± SD. Not Significant (N.S.); ** $p < 0.01$; *** $p < 0.005$; **** $p < 0.001$

LC-2 induced $KRAS^{G12C}$ degradation modulates Erk signaling in homozygous and heterozygous KRAS mutant cell lines

The ability of **LC-2** to modulate Erk signaling was investigated in NCI-H2030 and NCI-H23 cells during a 24 hour dose response. In NCI-H2030 cells, pErk was detected and a dose-dependent decrease in signaling was observed (Figure 5A). In addition, total Erk levels were elevated in a

dose-dependent manner. NCI-H23 cells showed a similar dose-dependent decrease in pErk (Figure 5B). Additionally, total Erk levels were elevated in a dose-dependent manner.

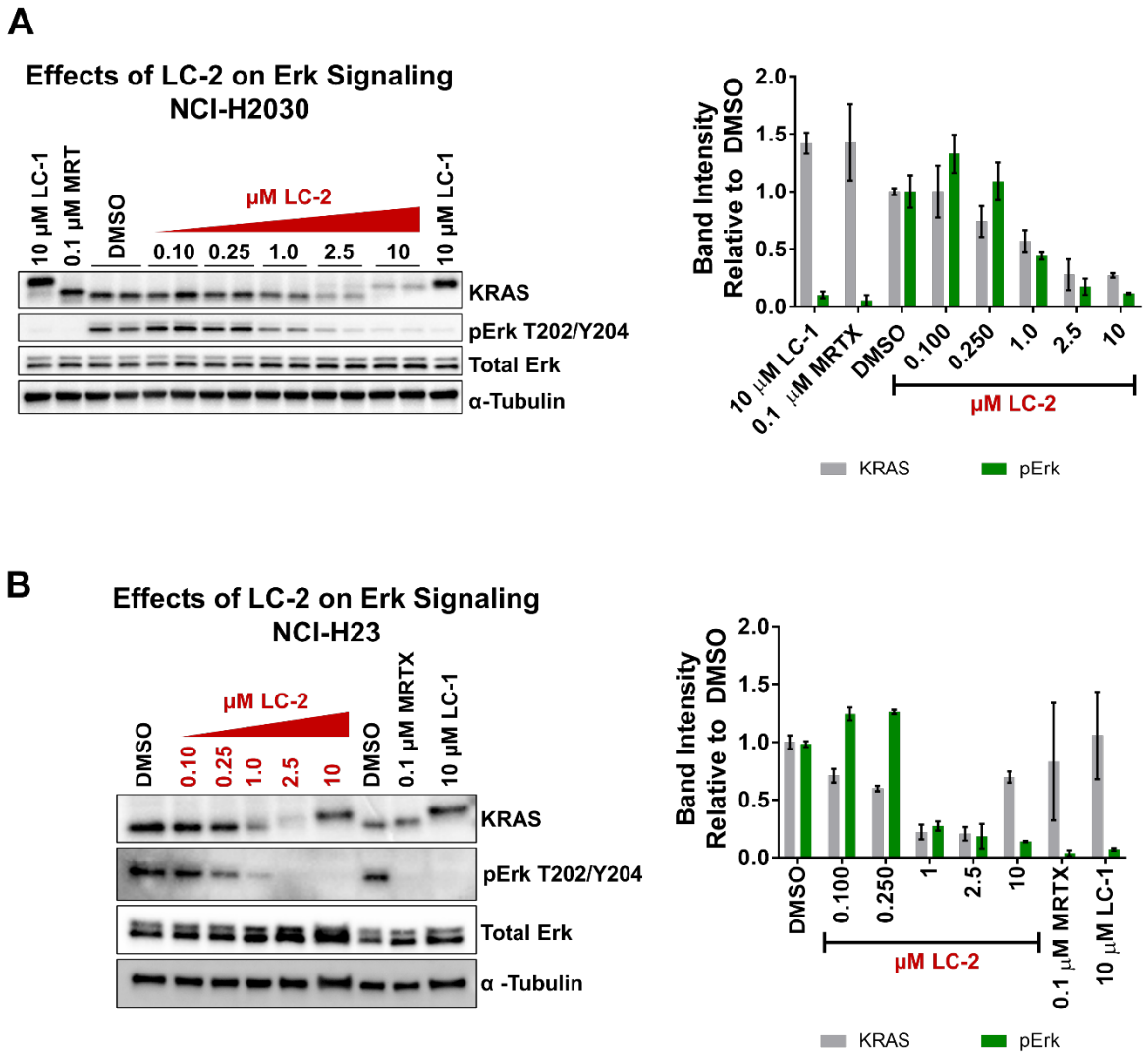

Figure 5: Degradation of endogenous KRASG12C modulates Erk signaling in homozygous and heterozygous KRASG12C cell lines. A) Degradation of KRASG12C in homozygous NCI-H2030 cells attenuates pErk in a dose dependent manner. Quantitation on the right. B) Degradation of KRASG12C in heterozygous NCI-H23 cells decreases pErk in a dose dependent manner. Quantitation on the right. For statistical analysis see Supplemental Tables 1 and 2. Quantified data represents mean ± SD.

Signaling kinetics were monitored during a 24 hour time course in MIA PaCa2, NCI-H23, and SW1573 cells treated with 2.5 μM **LC-2**. Modulation of Erk signaling by both **MRTX** and **LC-2** occurs within 6 hours in MIA PaCa-2 and NCI-H23 cells (Figure 6A-B and SI Figure 4). pErk was suppressed by both compounds at 6 and 24 hours in each cell lines. In SW1573 cells, phosphorylated Erk was inhibited by 2.5 μM **LC-2** between 1 and 4 hours, however pErk levels rebounded between 8 and 24 hours (SI Figure 4). Nonetheless, pErk levels were still significantly

lower in **LC-2** treated cells than DMSO treated cells at 24 hours. Total Erk was increased in **LC-2** treated cells compared to DMSO at all time points indicating the initiation of a positive feedback loop upon KRAS^{G12C} degradation and pErk inhibition. Taken together, these data show that **LC-2**-induced KRAS^{G12C} degradation is capable of modulating downstream signaling and that differences in signaling between inhibition and degradation are cell line dependent.

Discussion:

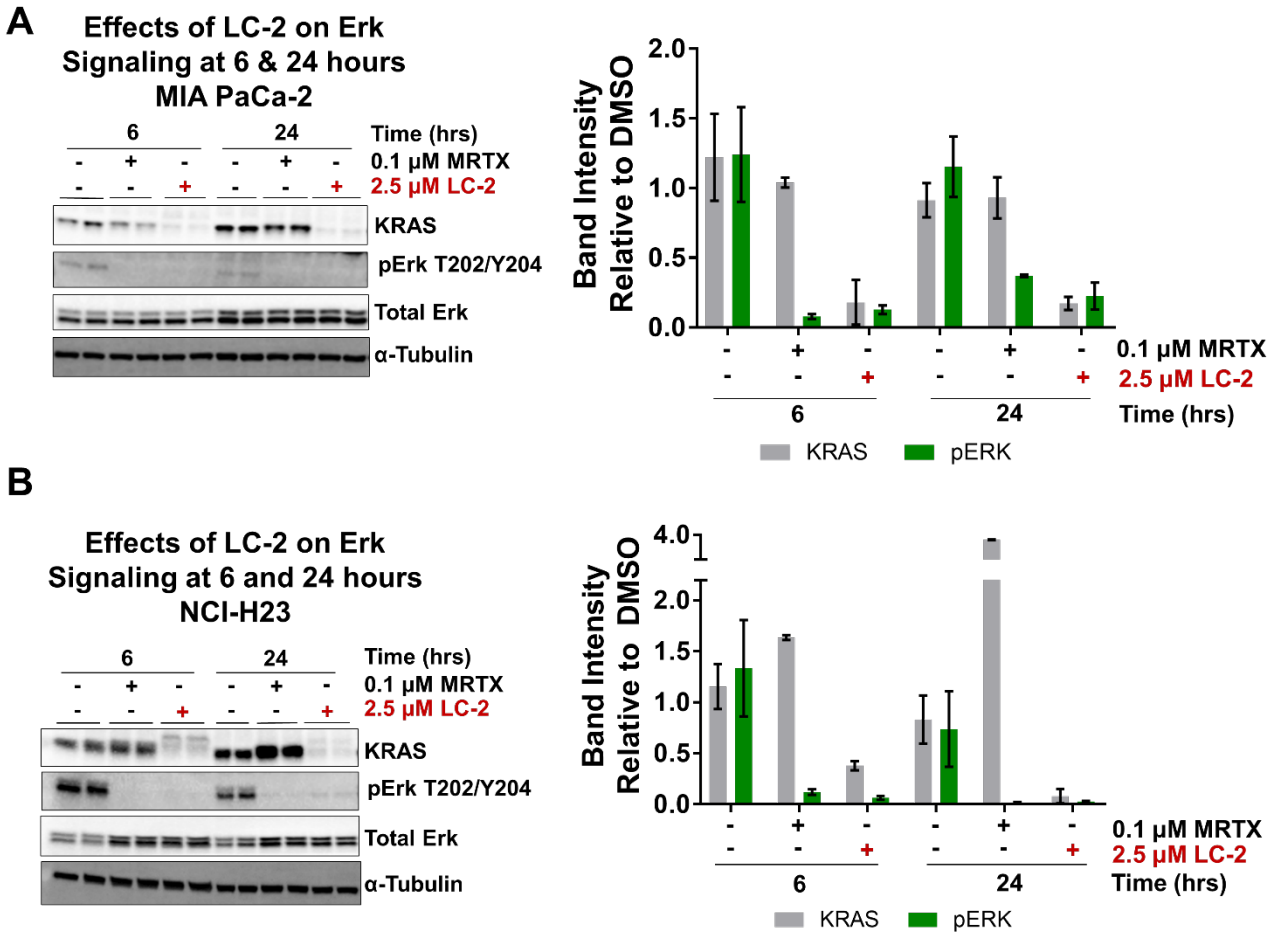

Figure 6: Effect of KRASG12C degradation and inhibition on Erk signaling over time. A) Inhibition and degradation of KRASG12C decreases pErk signaling at 6 and 24 hours in homozygous MIA PaCa-2 cells. Quantitation on the right. B) Inhibition and degradation of KRASG12C decreases pErk signaling at 6 and 24 hours in heterozygous NCI-H23. Quantitation on the right. For statistical analysis see Supplemental Tables 3 and 4. Quantified data represents mean ± SD.

To our knowledge, this study is the first report of PROTAC-induced endogenous KRAS^{G12C} degradation in cancer cells. Our PROTAC, **LC-2**, couples the covalent KRAS^{G12C} inhibitor **MRTX** to the VHL ligand developed in our laboratory[21, 39]. VHL recruitment to KRAS^{G12C} induces endogenous KRAS ubiquitination and degradation with DC_{50} values ranging from 0.25 to 0.76 μM. We observe

rapid engagement, sustained KRAS degradation, and attenuated pErk signaling for up to 72 hours in several $KRAS^{G12C}$ mutant cell lines. This tool compound will facilitate further exploration of how KRAS degradation influences downstream signaling and the viability of $KRAS^{G12C}$ mutant cancer cells with more precise temporal control than nucleic acid-based knockdown methods.

This work is not the first attempt at degrading $KRAS^{G12C}$. Recently, Zeng *et al.* were unsuccessful in degrading endogenous $KRAS^{G12C}$ with 20 μM of **XY-4-88** over 24 hours[38]. That PROTAC was based on **ARS1620** and used thalidomide to recruit cereblon, whereas our active PROTAC, **LC-2**, is **MRTX**-based and recruits VHL. It has been our observation that differences in either constituent ligand of a PROTAC can significantly impact the efficacy and selectivity of target engagement[31, 48]. Further studies will focus on understanding the importance of the $KRAS^{G12C}$ ligand, the recruited E3 ligase, or combination of the two factors in imparting **LC-2**'s activity. Conducting ternary complex assays by SPR and/or monitoring the ability of these compounds to induce ubiquitination by using tandem ubiquitin binding entity (TUBE) pulldowns followed by immunoblotting could address these questions[49].

With the availability of several new covalent inhibitors, kinome re-wiring in response to $KRAS^{G12C}$ inhibition has been an active research area. It has been found that signaling attenuated by **MRTX**, AMG510, and ARS1620 returns to or exceeds basal levels between 24 and 72 hours[21, 24-25]. This has been linked to the increased activity of several tyrosine kinases. To combat this acquired resistance, both targeted inhibition with FGFR inhibitors as well as pan-RTK inhibition with SHP2 inhibitors in combination with $KRAS^{G12C}$ inhibition have been successfully used to reduce the recovery of inhibited signaling[24]. These co-treatment regimens have also been shown to be more anti-proliferative *in vitro* and *in vivo* compared to RTK inhibition or $KRAS^{G12C}$ inhibition alone[24, 50]. It will be interesting to determine whether degradation alone can overcome Erk signaling reactivation and/or if combination of KRAS degradation with RTK inhibition could further enhance antiproliferative effects. In addition to the re-wiring of sensitive cells, there are known cell lines, such as SW1573 (used in this work) and NCI-H1792, that are inherently resistant to the anti-proliferative effects of $KRAS^{G12C}$ inhibition. Recently, it was shown that siRNA mediated knockdown in these cells, but not $KRAS^{G12C}$ inhibition, resulted in ~50% decreased cell viability[50]. Therefore, it will be interesting to determine if $KRAS^{G12C}$-induced degradation of $KRAS^{G12C}$ by **LC-2** is also similarly antiproliferative in these cell lines.

The ability to target KRAS with covalent inhibitors was itself a milestone in drug discovery. It showed that proteins formally deemed undruggable could be targeted with small molecules. Similarly, the results presented here demonstrate that endogenous $KRAS^{G12C}$ can be degraded as

long as a suitable ligand is identified. While ligand development for other KRAS mutants continues, **LC-2** can serve as a tool compound to investigate biology in the context of rapid $KRAS^{G12C}$ degradation, i.e., cell viability. One caveat with our lead compound **LC-2** is that the covalent nature of the PROTAC may limit its potency as it cannot participate in catalytic rounds of degradation[30]. Therefore, efforts to develop reversible PROTACs to target KRAS mutants are warranted. Despite its limitations, the discovery of **LC-2** opens new opportunities for targeting KRAS mutants in cancer therapy.

Acknowledgements:

We would like to thank Dr. Saul Jaime-Figueroa for assisting with the MRTX849 docking. We would also like to thank Dr. Kanak Raina for his helpful comments in the project. Finally, we would like to thank Dr. John Hines for his insight, comments and critiques in the preparation of this manuscript. C.M.C. is funded by the NIH (R35CA197589) and is supported by an American Cancer Research Professorship. M.J.B acknowledges support from the NIH (F31CA232477 and 5T32GM067543).

Declaration of Competing Interests:

The authors declare the following competing financial interest(s): C.M.C is founder, shareholder, and consultant to Arvinas, Inc., which supports research in his laboratory.

References:

1. Prior, I. A.; Lewis, P. D.; Mattos, C., A comprehensive survey of Ras mutations in cancer. *Cancer Res* **2012,** *72* (10), 2457-67.
2. Land, H.; Parada, L. F.; Weinberg, R. A., Tumorigenic conversion of primary embryo fibroblasts requires at least two cooperating oncogenes. *Nature* **1983,** *304* (5927), 596-602.
3. Newbold, R. F.; Overell, R. W., Fibroblast Immortality Is a Prerequisite for Transformation by Ej C-Ha-Ras Oncogene. *Nature* **1983,** *304* (5927), 648-651.
4. Milburn, M. V.; Tong, L.; Devos, A. M.; Brunger, A.; Yamaizumi, Z.; Nishimura, S.; Kim, S. H., Molecular Switch for Signal Transduction - Structural Differences between Active and Inactive Forms of Protooncogenic Ras Proteins. *Science* **1990,** *247* (4945), 939-945.
5. Simanshu, D. K.; Nissley, D. V.; McCormick, F., RAS Proteins and Their Regulators in Human Disease. *Cell* **2017,** *170* (1), 17-33.
6. Ito, Y.; Yamasaki, K.; Iwahara, J.; Terada, T.; Kamiya, A.; Shirouzu, M.; Muto, Y.; Kawai, G.; Yokoyama, S.; Laue, E. D.; Walchli, M.; Shibata, T.; Nishimura, S.; Miyazawa, T., Regional

polysterism in the GTP-bound form of the human c-Ha-Ras protein. *Biochemistry* **1997,** *36* (30), 9109-9119.
7. Bar-Sagi, D., The Sos (Son of sevenless) protein. *Trends Endocrinol Metab* **1994,** *5* (4), 165-9.
8. Pierre, S.; Bats, A. S.; Coumoul, X., Understanding SOS (Son of Sevenless). *Biochem Pharmacol* **2011,** *82* (9), 1049-56.
9. Harrell Stewart, D. R.; Clark, G. J., Pumping the brakes on RAS - negative regulators and death effectors of RAS. *J Cell Sci* **2020,** *133* (3).
10. Boriack-Sjodin, P. A.; Margarit, S. M.; Bar-Sagi, D.; Kuriyan, J., The structural basis of the activation of Ras by Sos. *Nature* **1998,** *394* (6691), 337-43.
11. Scheffzek, K.; Ahmadian, M. R.; Kabsch, W.; Wiesmuller, L.; Lautwein, A.; Schmitz, F.; Wittinghofer, A., The Ras-RasGAP complex: structural basis for GTPase activation and its loss in oncogenic Ras mutants. *Science* **1997,** *277* (5324), 333-8.
12. Spencer-Smith, R.; O'Bryan, J. P., Direct inhibition of RAS: Quest for the Holy Grail? *Semin Cancer Biol* **2019,** *54*, 138-148.
13. Campbell, J. D.; Alexandrov, A.; Kim, J.; Wala, J.; Berger, A. H.; Pedamallu, C. S.; Shukla, S. A.; Guo, G.; Brooks, A. N.; Murray, B. A.; Imielinski, M.; Hu, X.; Ling, S.; Akbani, R.; Rosenberg, M.; Cibulskis, C.; Ramachandran, A.; Collisson, E. A.; Kwiatkowski, D. J.; Lawrence, M. S.; Weinstein, J. N.; Verhaak, R. G.; Wu, C. J.; Hammerman, P. S.; Cherniack, A. D.; Getz, G.; Cancer Genome Atlas Research, N.; Artyomov, M. N.; Schreiber, R.; Govindan, R.; Meyerson, M., Distinct patterns of somatic genome alterations in lung adenocarcinomas and squamous cell carcinomas. *Nat Genet* **2016,** *48* (6), 607-16.
14. Lu, S.; Banerjee, A.; Jang, H.; Zhang, J.; Gaponenko, V.; Nussinov, R., GTP Binding and Oncogenic Mutations May Attenuate Hypervariable Region (HVR)-Catalytic Domain Interactions in Small GTPase K-Ras4B, Exposing the Effector Binding Site. *J Biol Chem* **2015,** *290* (48), 28887-900.
15. Ostrem, J. M.; Peters, U.; Sos, M. L.; Wells, J. A.; Shokat, K. M., K-Ras(G12C) inhibitors allosterically control GTP affinity and effector interactions. *Nature* **2013,** *503* (7477), 548-51.
16. Rudolph, J.; Stokoe, D., Selective inhibition of mutant Ras protein through covalent binding. *Angew Chem Int Ed Engl* **2014,** *53* (15), 3777-9.
17. Ostrem, J. M.; Shokat, K. M., Direct small-molecule inhibitors of KRAS: from structural insights to mechanism-based design. *Nat Rev Drug Discov* **2016,** *15* (11), 771-785.
18. Nnadi, C. I.; Jenkins, M. L.; Gentile, D. R.; Bateman, L. A.; Zaidman, D.; Balius, T. E.; Nomura, D. K.; Burke, J. E.; Shokat, K. M.; London, N., Novel K-Ras G12C Switch-II Covalent Binders Destabilize Ras and Accelerate Nucleotide Exchange. *J Chem Inf Model* **2018,** *58* (2), 464-471.
19. Janes, M. R.; Zhang, J.; Li, L. S.; Hansen, R.; Peters, U.; Guo, X.; Chen, Y.; Babbar, A.; Firdaus, S. J.; Darjania, L.; Feng, J.; Chen, J. H.; Li, S.; Li, S.; Long, Y. O.; Thach, C.; Liu, Y.; Zarieh, A.; Ely, T.; Kucharski, J. M.; Kessler, L. V.; Wu, T.; Yu, K.; Wang, Y.; Yao, Y.; Deng, X.; Zarrinkar, P. P.; Brehmer, D.; Dhanak, D.; Lorenzi, M. V.; Hu-Lowe, D.; Patricelli, M. P.; Ren, P.; Liu, Y., Targeting KRAS Mutant Cancers with a Covalent G12C-Specific Inhibitor. *Cell* **2018,** *172* (3), 578-589 e17.
20. Canon, J.; Rex, K.; Saiki, A. Y.; Mohr, C.; Cooke, K.; Bagal, D.; Gaida, K.; Holt, T.; Knutson, C. G.; Koppada, N.; Lanman, B. A.; Werner, J.; Rapaport, A. S.; San Miguel, T.; Ortiz, R.; Osgood, T.; Sun, J. R.; Zhu, X.; McCarter, J. D.; Volak, L. P.; Houk, B. E.; Fakih, M. G.; O'Neil, B. H.; Price, T. J.; Falchook, G. S.; Desai, J.; Kuo, J.; Govindan, R.; Hong, D. S.; Ouyang, W.; Henary, H.; Arvedson, T.; Cee, V. J.; Lipford, J. R., The clinical KRAS(G12C) inhibitor AMG 510 drives anti-tumour immunity. *Nature* **2019,** *575* (7781), 217-223.
21. Hallin, J.; Engstrom, L. D.; Hargis, L.; Calinisan, A.; Aranda, R.; Briere, D. M.; Sudhakar, N.; Bowcut, V.; Baer, B. R.; Ballard, J. A.; Burkard, M. R.; Fell, J. B.; Fischer, J. P.; Vigers, G. P.; Xue, Y.; Gatto, S.; Fernandez-Banet, J.; Pavlicek, A.; Velastagui, K.; Chao, R. C.; Barton, J.;

Pierobon, M.; Baldelli, E.; Patricoin, E. F., 3rd; Cassidy, D. P.; Marx, M. A.; Rybkin, II; Johnson, M. L.; Ou, S. I.; Lito, P.; Papadopoulos, K. P.; Janne, P. A.; Olson, P.; Christensen, J. G., The KRAS(G12C) Inhibitor MRTX849 Provides Insight toward Therapeutic Susceptibility of KRAS-Mutant Cancers in Mouse Models and Patients. *Cancer Discov* **2020,** *10* (1), 54-71.

22. Race for undruggable KRAS speeds up. *Nat Biotechnol* **2019,** *37* (11), 1247.
23. Seton-Rogers, S., KRAS-G12C in the crosshairs. *Nat Rev Cancer* **2020,** *20* (1), 3.
24. Ryan, M. B.; Fece de la Cruz, F.; Phat, S.; Myers, D. T.; Wong, E.; Shahzade, H. A.; Hong, C. B.; Corcoran, R. B., Vertical Pathway Inhibition Overcomes Adaptive Feedback Resistance to KRAS(G12C) Inhibition. *Clin Cancer Res* **2019**.
25. Xue, J. Y.; Zhao, Y.; Aronowitz, J.; Mai, T. T.; Vides, A.; Qeriqi, B.; Kim, D.; Li, C.; de Stanchina, E.; Mazutis, L.; Risso, D.; Lito, P., Rapid non-uniform adaptation to conformation-specific KRAS(G12C) inhibition. *Nature* **2020,** *577* (7790), 421-425.
26. Sakamoto, K. M.; Kim, K. B.; Kumagai, A.; Mercurio, F.; Crews, C. M.; Deshaies, R. J., Protacs: Chimeric molecules that target proteins to the Skp1-Cullin-F box complex for ubiquitination and degradation. *P Natl Acad Sci USA* **2001,** *98* (15), 8554-8559.
27. Burslem, G. M.; Crews, C. M., Proteolysis-Targeting Chimeras as Therapeutics and Tools for Biological Discovery. *Cell* **2020**.
28. Paiva, S. L.; Crews, C. M., Targeted protein degradation: elements of PROTAC design. *Curr Opin Chem Biol* **2019,** *50*, 111-119.
29. Pettersson, M.; Crews, C. M., PROteolysis TArgeting Chimeras (PROTACs) - Past, present and future. *Drug Discov Today Technol* **2019,** *31*, 15-27.
30. Bondeson, D. P.; Mares, A.; Smith, I. E. D.; Ko, E.; Campos, S.; Miah, A. H.; Mulholland, K. E.; Routly, N.; Buckley, D. L.; Gustafson, J. L.; Zinn, N.; Grandi, P.; Shimamura, S.; Bergamini, G.; Faelth-Savitski, M.; Bantscheff, M.; Cox, C.; Gordon, D. A.; Willard, R. R.; Flanagan, J. J.; Casillas, L. N.; Votta, B. J.; den Besten, W.; Famm, K.; Kruidenier, L.; Carter, P. S.; Harling, J. D.; Churcher, I.; Crews, C. M., Catalytic in vivo protein knockdown by small-molecule PROTACs. *Nat Chem Biol* **2015,** *11* (8), 611-U120.
31. Bondeson, D. P.; Smith, B. E.; Burslem, G. M.; Buhimschi, A. D.; Hines, J.; Jaime-Figueroa, S.; Wang, J.; Hamman, B. D.; Ishchenko, A.; Crews, C. M., Lessons in PROTAC Design from Selective Degradation with a Promiscuous Warhead. *Cell Chemical Biology* **2018,** *25* (1), 78-+.
32. Burslem, G. M.; Smith, B. E.; Lai, A. C.; Jaime-Figueroa, S.; McQuaid, D. C.; Bondeson, D. P.; Toure, M.; Dong, H. Q.; Qian, Y. M.; Wang, J.; Crew, A. P.; Hines, J.; Crews, C. M., The Advantages of Targeted Protein Degradation Over Inhibition: An RTK Case Study. *Cell Chemical Biology* **2018,** *25* (1), 67-+.
33. Salami, J.; Alabi, S.; Willard, R. R.; Vitale, N. J.; Wang, J.; Dong, H. Q.; Jin, M. Z.; McDonnell, D. P.; Crew, A. P.; Neklesa, T. K.; Crews, C. M., Androgen receptor degradation by the proteolysis-targeting chimera ARCC-4 outperforms enzalutamide in cellular models of prostate cancer drug resistance. *Commun Biol* **2018,** *1*.
34. Cromm, P. M.; Samarasinghe, K. T. G.; Hines, J.; Crews, C. M., Addressing Kinase-Independent Functions of Fak via PROTAC-Mediated Degradation. *J Am Chem Soc* **2018,** *140* (49), 17019-17026.
35. Burslem, G. M.; Song, J. Y.; Chen, X.; Hines, J.; Crews, C. M., Enhancing Antiproliferative Activity and Selectivity of a FLT-3 Inhibitor by Proteolysis Targeting Chimera Conversion. *J Am Chem Soc* **2018,** *140* (48), 16428-16432.
36. Burslem, G. M.; Schultz, A. R.; Bondeson, D. P.; Eide, C. A.; Stevens, S. L. S.; Druker, B. J.; Crews, C. M., Targeting BCR-ABL1 in Chronic Myeloid Leukemia by PROTAC-Mediated Targeted Protein Degradation. *Cancer Research* **2019,** *79* (18), 4744-4753.

37. Ito, T.; Ando, H.; Suzuki, T.; Ogura, T.; Hotta, K.; Imamura, Y.; Yamaguchi, Y.; Handa, H., Identification of a Primary Target of Thalidomide Teratogenicity. *Science* **2010,** *327* (5971), 1345-1350.
38. Zeng, M.; Xiong, Y.; Safaee, N.; Nowak, R. P.; Donovan, K. A.; Yuan, C. J.; Nabet, B.; Gero, T. W.; Feru, F.; Li, L.; Gondi, S.; Ombelets, L. J.; Quan, C.; Janne, P. A.; Kostic, M.; Scott, D. A.; Westover, K. D.; Fischer, E. S.; Gray, N. S., Exploring Targeted Degradation Strategy for Oncogenic KRAS(G12C). *Cell Chem Biol* **2020,** *27* (1), 19-31 e6.
39. Buckley, D. L.; Van Molle, I.; Gareiss, P. C.; Tae, H. S.; Michel, J.; Noblin, D. J.; Jorgensen, W. L.; Ciulli, A.; Crews, C. M., Targeting the von Hippel-Lindau E3 Ubiquitin Ligase Using Small Molecules To Disrupt the VHL/HIF-1 alpha Interaction. *J Am Chem Soc* **2012,** *134* (10), 4465-4468.
40. Buckley, D. L.; Raina, K.; Darricarrere, N.; Hines, J.; Gustafson, J. L.; Smith, I. E.; Miah, A. H.; Harling, J. D.; Crews, C. M., HaloPROTACS: Use of Small Molecule PROTACs to Induce Degradation of HaloTag Fusion Proteins. *Acs Chem Biol* **2015,** *10* (8), 1831-7.
41. Sunaga, N.; Shames, D. S.; Girard, L.; Peyton, M.; Larsen, J. E.; Imai, H.; Soh, J.; Sato, M.; Yanagitani, N.; Kaira, K.; Xie, Y.; Gazdar, A. F.; Mori, M.; Minna, J. D., Knockdown of oncogenic KRAS in non-small cell lung cancers suppresses tumor growth and sensitizes tumor cells to targeted therapy. *Mol Cancer Ther* **2011,** *10* (2), 336-46.
42. Merlet, J.; Burger, J.; Gomes, J. E.; Pintard, L., Regulation of cullin-RING E3 ubiquitin-ligases by neddylation and dimerization. *Cell Mol Life Sci* **2009,** *66* (11-12), 1924-38.
43. Meng, L.; Mohan, R.; Kwok, B. H.; Elofsson, M.; Sin, N.; Crews, C. M., Epoxomicin, a potent and selective proteasome inhibitor, exhibits in vivo antiinflammatory activity. *Proc Natl Acad Sci U S A* **1999,** *96* (18), 10403-8.
44. Soucy, T. A.; Smith, P. G.; Milhollen, M. A.; Berger, A. J.; Gavin, J. M.; Adhikari, S.; Brownell, J. E.; Burke, K. E.; Cardin, D. P.; Critchley, S.; Cullis, C. A.; Doucette, A.; Garnsey, J. J.; Gaulin, J. L.; Gershman, R. E.; Lublinsky, A. R.; McDonald, A.; Mizutani, H.; Narayanan, U.; Olhava, E. J.; Peluso, S.; Rezaei, M.; Sintchak, M. D.; Talreja, T.; Thomas, M. P.; Traore, T.; Vyskocil, S.; Weatherhead, G. S.; Yu, J.; Zhang, J.; Dick, L. R.; Claiborne, C. F.; Rolfe, M.; Bolen, J. B.; Langston, S. P., An inhibitor of NEDD8-activating enzyme as a new approach to treat cancer. *Nature* **2009,** *458* (7239), 732-U67.
45. Lu, A.; Tebar, F.; Alvarez-Moya, B.; Lopez-Alcala, C.; Calvo, M.; Enrich, C.; Agell, N.; Nakamura, T.; Matsuda, M.; Bachs, O., A clathrin-dependent pathway leads to KRas signaling on late endosomes en route to lysosomes. *J Cell Biol* **2009,** *184* (6), 863-879.
46. Oda, K.; Nishimura, Y.; Ikehara, Y.; Kato, K., Bafilomycin-A1 Inhibits the Targeting of Lysosomal Acid-Hydrolases in Cultured-Hepatocytes. *Biochem Bioph Res Co* **1991,** *178* (1), 369-377.
47. Lu, J.; Qian, Y.; Altieri, M.; Dong, H.; Wang, J.; Raina, K.; Hines, J.; Winkler, J. D.; Crew, A. P.; Coleman, K.; Crews, C. M., Hijacking the E3 Ubiquitin Ligase Cereblon to Efficiently Target BRD4. *Chem Biol* **2015,** *22* (6), 755-63.
48. Lai, A. C.; Toure, M.; Hellerschmied, D.; Salami, J.; Jaime-Figueroa, S.; Ko, E.; Hines, J.; Crews, C. M., Modular PROTAC Design for the Degradation of Oncogenic BCR-ABL. *Angew Chem Int Ed Engl* **2016,** *55* (2), 807-10.
49. Hjerpe, R.; Aillet, F.; Lopitz-Otsoa, F.; Lang, V.; England, P.; Rodriguez, M. S., Efficient protection and isolation of ubiquitylated proteins using tandem ubiquitin-binding entities. *Embo Rep* **2009,** *10* (11), 1250-1258.
50. Misale, S.; Fatherree, J. P.; Cortez, E.; Li, C.; Bilton, S.; Timonina, D.; Myers, D. T.; Lee, D.; Gomez-Caraballo, M.; Greenberg, M.; Nangia, V.; Greninger, P.; Egan, R. K.; McClanaghan, J.; Stein, G. T.; Murchie, E.; Zarrinkar, P. P.; Janes, M. R.; Li, L. S.; Liu, Y.; Hata, A. N.; Benes, C. H., KRAS G12C NSCLC Models Are Sensitive to Direct Targeting of KRAS in Combination with PI3K Inhibition. *Clin Cancer Res* **2019,** *25* (2), 796-807.

4.5.2020.KRAS PROTAC Paper Draft v9.1 CMC.docx (4.16 MiB) view on ChemRxiv • download file

A

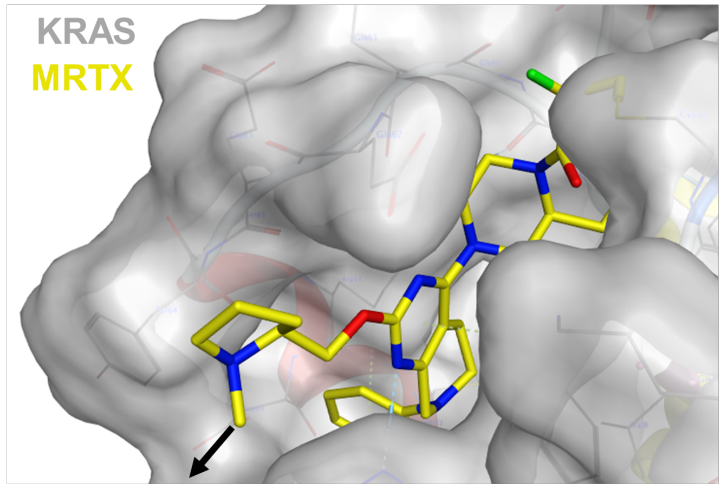
KRAS
MRTX

B

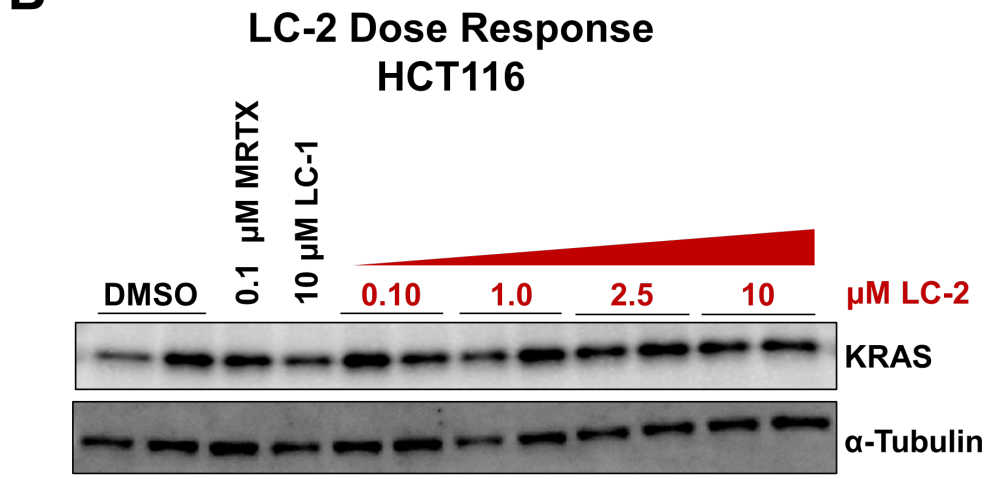
LC-2 Dose Response
HCT116
DMSO
0.1 μM MRTX
10 μM LC-1
0.10
1.0
2.5
10
μM LC-2
KRAS
α-Tubulin

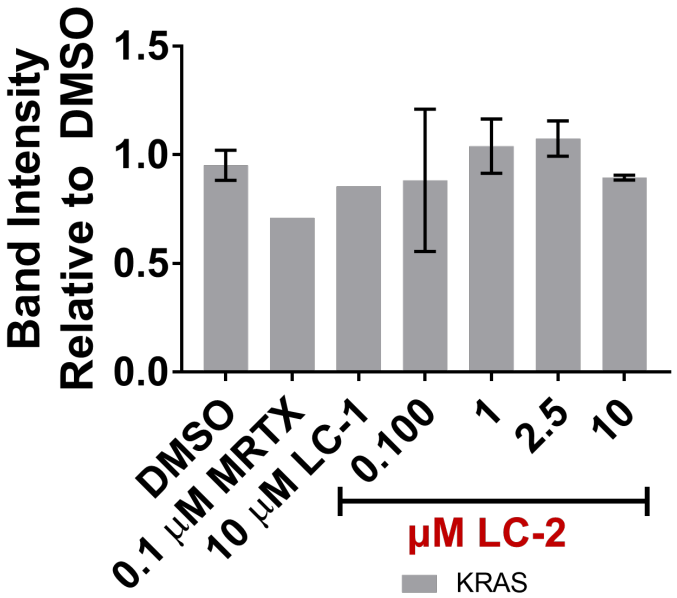
Band Intensity
Relative to DMSO
1.5
1.0
0.5
0.0
DMSO
0.1 μM MRTX
10 μM LC-1
0.100
1
2.5
10
μM LC-2
KRAS

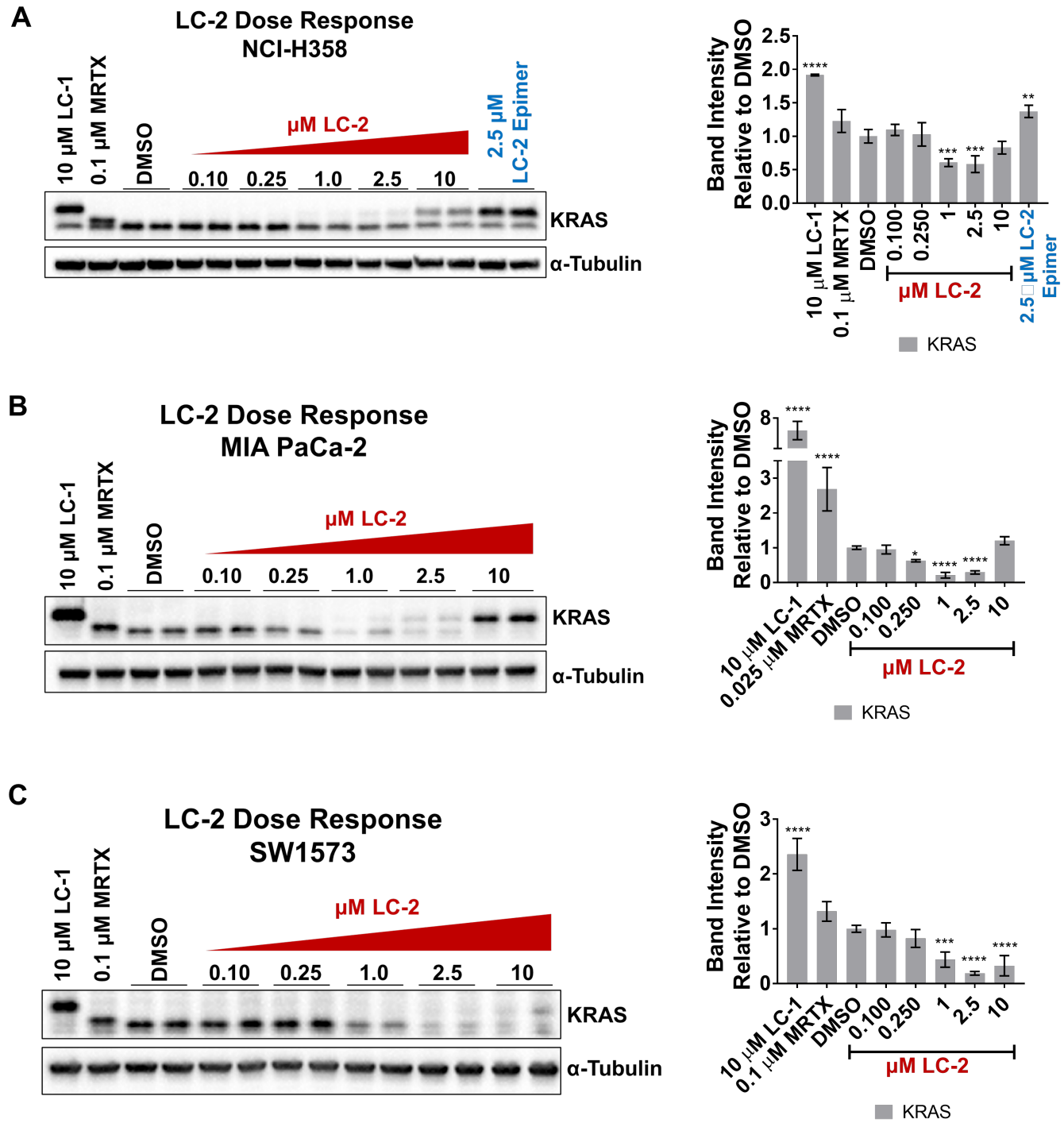
A
LC-2 Dose Response
NCI-H358
10 µM LC-1
0.1 µM MRTX
DMSO
µM LC-2
0.10
0.25
1.0
2.5
10
2.5 µM LC-2 Epimer
KRAS
α-Tubulin
Band Intensity Relative to DMSO
B
LC-2 Dose Response
MIA PaCa-2
0.025 µM MRTX
C
LC-2 Dose Response
SW1573

Extended MRTX, LC-2, and LC-2 Epimer Time Course SW1573

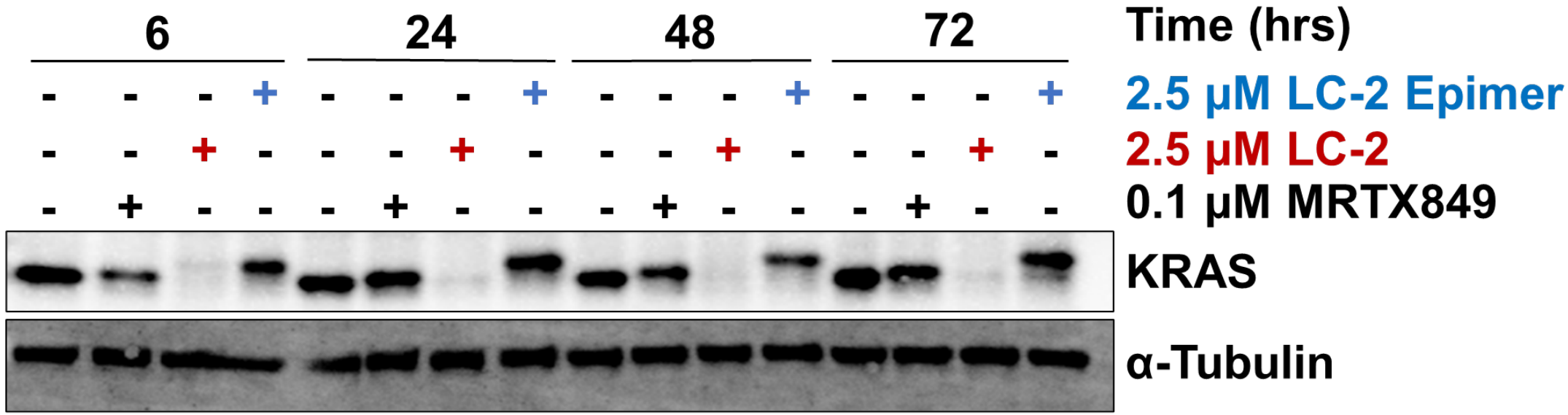

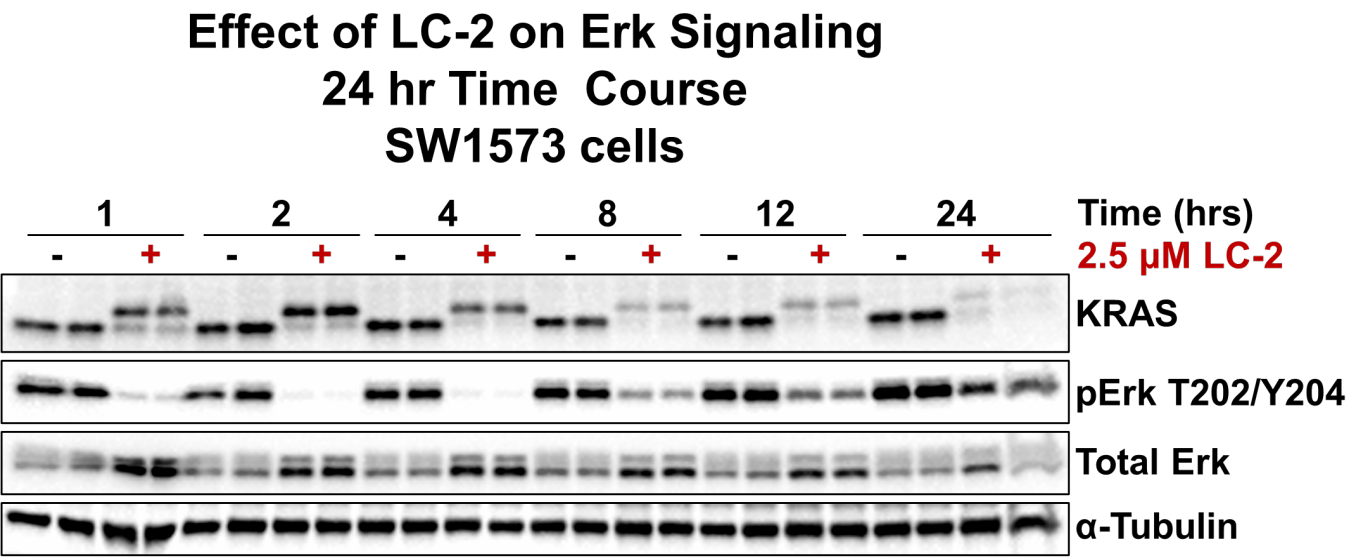
Effect of LC-2 on Erk Signaling
24 hr Time Course
SW1573 cells
1
2
4
8
12
24
Time (hrs)
- + - + - + - + - + - +
2.5 μM LC-2
KRAS
pErk T202/Y204
Total Erk
α-Tubulin

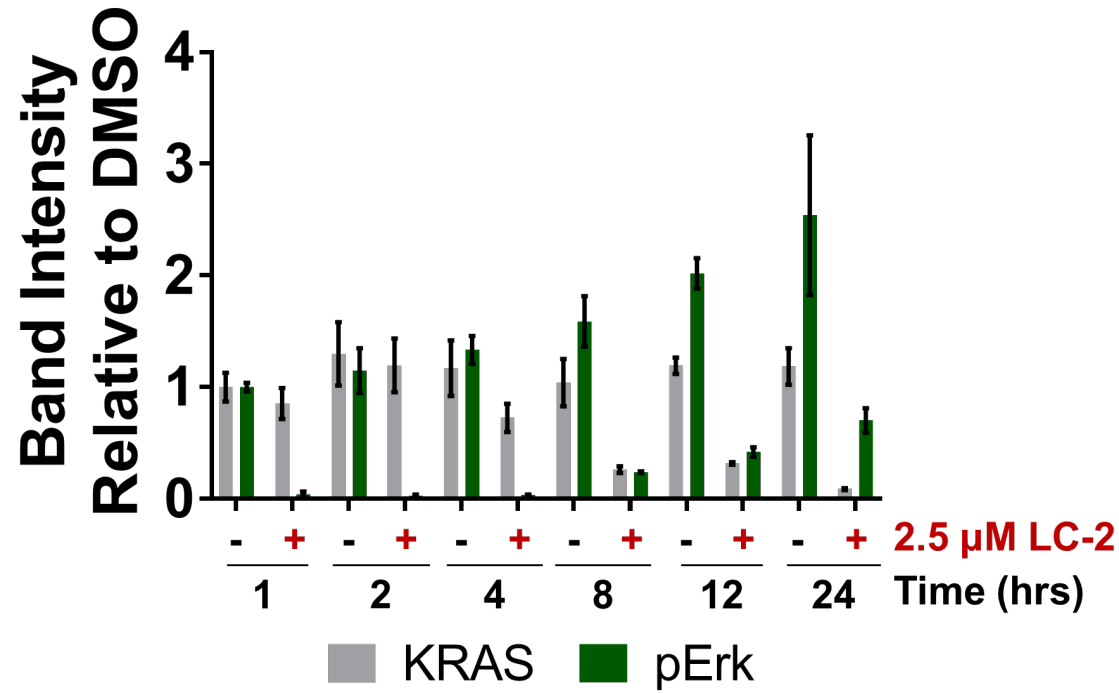
Band Intensity
Relative to DMSO
0
1
2
3
4
- + - + - + - + - + - +
2.5 μM LC-2
1
2
4
8
12
24
Time (hrs)
KRAS
pErk

Effects of LC-2 on Erk Signaling
NCI-H2030

	DMSO	10 μM LC-1	100 nM MRTX849	0.1 μM LC-2	0.25 μM LC-2	1.0 μM LC-2	2.5 μM LC-2	10 μM LC-2
KRAS	N/A	*	*	N.S	N.S	**	****	****
pErk	N/A	****	****	*	N.S	****	****	****

SI Table 1: Two-way ANOVA analysis of Figure 5A. Not Significant (N.S.); * $p < 0.05$; $p < 0.001$.

Effects of LC-2 on Erk Signaling
NCI-H23

	DMSO	0.1 μM LC-2	0.25 μM LC-2	1.0 μM LC-2	2.5 μM LC-2	10 μM LC-2	100 nM MRTX849	10 μM LC-1
KRAS	N/A	N.S.	*	****	*****	N.S.	N.S.	N.S.
pErk	N/A	N.S.	N.S.	N.S.	*	N.S.	*	*

SI Table 2: Two-way ANOVA analysis of Figure 5B. Not Significant (N.S.); * $p < 0.05$; ** $p < 0.01$.

Effects of LC-2 on Erk Signaling at 6 and 24 hours MIA PaCa-2

	Time (hrs)					
	6			24		
	DMSO	100 nM MRTX849	2.5 μM LC-2	DMSO	100 nM MRTX849	2.5 μM LC-2
KRAS	N/A	N.S	**	N.S	N.S	**
pErk	N/A	****	**	N.S	*	**

SI Table 3: Two-way ANOVA analysis of Figure 6A**.** Not Significant (N.S.); * $p < 0.05$; ** $p < 0.01$; **** $p < 0.001$.

Effects of LC-2 on KRAS Signaling at 6 and 24 hours NCI-H23

	Time (hrs)					
	6			24		
	DMSO	100 nM MRTX849	2.5 μM LC-2	DMSO	100 nM MRTX849	2.5 μM LC-2
KRAS	N/A	N.S	**	N.S	****	****
pErk	N/A	****	****	*	****	****

SI Table 4: Two-way ANOVA analysis of Figure 6B. Not Significant (N.S.); * $p < 0.05$; ** $p < 0.01$; **** $p < 0.001$.

Effect of LC-2 on KRAS Signaling
24 hour Time Course
SW1573 cells

	Time (hrs)											
	1		2		4		8		12		24	
	DMSO	2.5 μM LC-2	DMSO	2.5 μM LC-2	DMSO	2.5 μM LC-2	DMSO	2.5 μM LC-2	DMSO	2.5 μM LC-2	DMSO	2.5 μM LC-2
KRAS	N/A	N.S.	N.S.	N.S.	N.S.	N.S	N.S.	**	N.S.	**	N.S.	***
pErk	N/A	****	N.S.	****	N.S.	****	*	**	****	*	****	N.S

SI Table 5: Two-way ANOVA analysis of SI Figure 4. Not Significant (N.S.); * $p < 0.05$; ** $p < 0.01$; *** $p < 0.005$; $p < 0.001$.

KRAS Supplemental Figures Final v2.pdf (4.69 MiB) view on ChemRxiv • download file

Supporting Information

Targeted Degradation of Oncogenic KRAS^{G12C} by VHL Recruiting PROTACs

Michael J. Bond[1, †], Ling Chu[2, †], Dhanusha A. Nalawansha[2], Ke Li[2], Craig M. Crews[*,1,2,3]

*Corresponding Author; e-mail:craig.crews@yale.edu

[1]Department of Pharmacology, Yale University, New Haven, Connecticut 06511, United States

[2]Department of Molecular, Cellular, and Developmental Biology, Yale University, 260 Whitney Avenue, New Haven, Connecticut, 06511, United States

[3]Department of Chemistry, Yale University, New Haven, Connecticut 06511, United States

[†]These authors contributed equally to this work

20 Pages

Supporting Information Figures 1-4

Supporting Information Tables 1-5

Materials and Methods

Chemical Synthesis

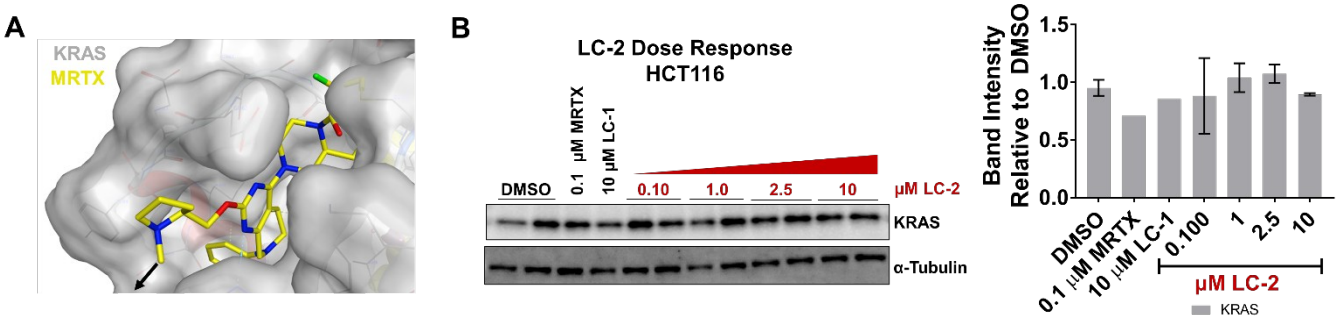

Supporting Information Figure 1: Docking of MRTX849 and LC-2 degradation is specific for KRAS^{G12C}. A) Docking of MRTX849 (MRTX) into the crystal structure of KRAS^{G12C} (PDB: 5V9U). MRTX is shown in yellow, the black arrow indicates the point of linker attachment. B) LC-2 does not degrade KRAS^{G12D} in HCT116 cells. Quantitation on the right. Quantitation on the right. Quantified data represents mean ± SD.

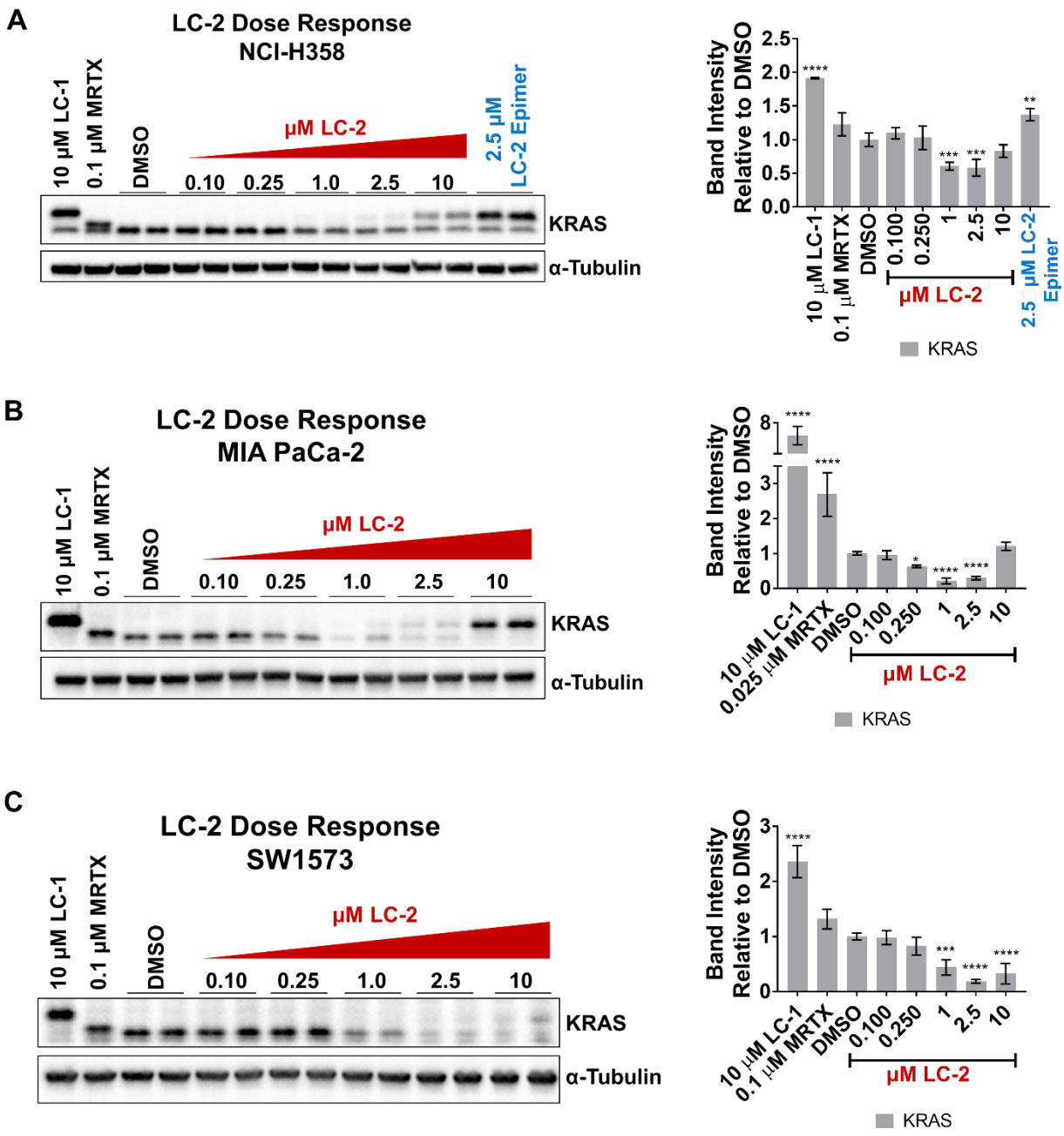

Supporting Information Figure 2: LC-2 induces KRAS^{G12C} degradation in multiple mutant cell lines. A) LC-2, but not LC-2 Epimer, induces KRAS^{G12C} degradation in heterozygous H358 cells. Quantitation on the right. B) LC-2 induces KRAS^{G12C} in homozygous MIA PaCa-2 cells. Quantitation on the right. C) LC-2 induces KRAS^{G12C} degradation in the homozygous, MRTX849 resistant, SW1573 cells. Quantitation on the right. Quantified data represents mean ± SD. * $p < 0.05$; ** $p < 0.01$; *** $p < 0.005$; **** $p < 0.001$

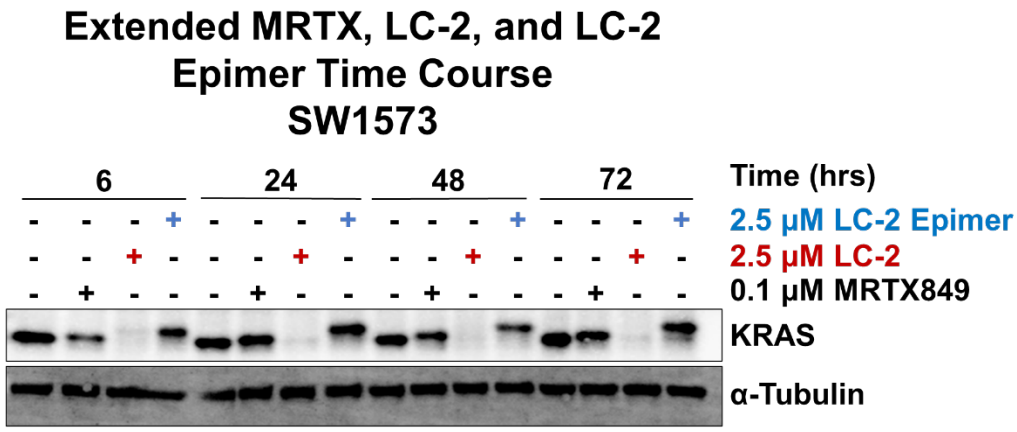

Supporting Information Figure 3: LC-2 induced KRAS^{G12C} degradation is maintained over 72 hours in SW1573. LC-2 induced KRAS^{G12C} occurs within 6 hrs and is maintained for 72 hours. No change is observed for LC-2 Epimer.

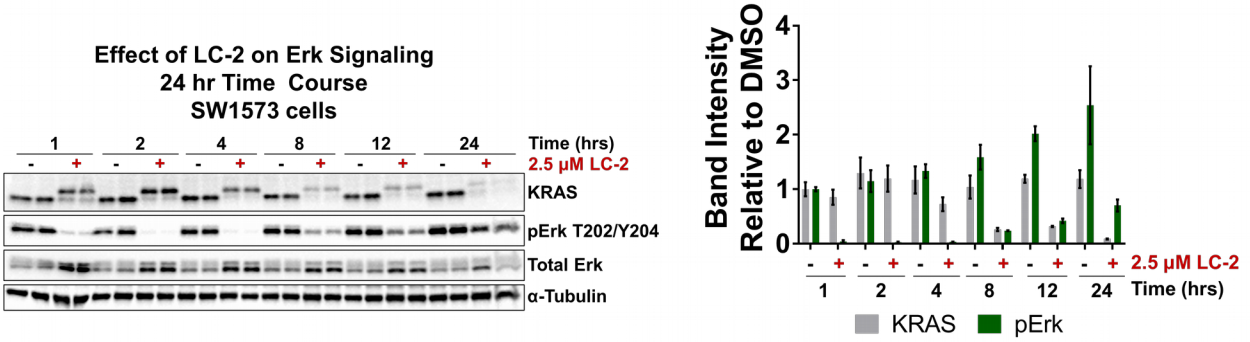

Supporting Information Figure 4: Changes in Erk signaling during a 24 hour LC-2 treatment in SW1573 cells. Erk signaling is modulated by LC-2. pErk is decreased throughout the time course. Quantitation on the right. Quantified data represents mean ± SD. For statistical analysis see SI table 5.

Effects of LC-2 on Erk Signaling
NCI-H2030

	DMSO	10 μM LC-1	100 nM MRTX849	0.1 μM LC-2	0.25 μM LC-2	1.0 μM LC-2	2.5 μM LC-2	10 μM LC-2
KRAS	N/A	*	*	N.S	N.S	**	****	****
pErk	N/A	****	****	*	N.S	****	****	****

Supporting Information Table 1: Two-way ANOVA analysis of Figure 5A. Not Significant (N.S.); * $p < 0.05$; ** $p < 0.01$; **** $p < 0.001$.

Effects of LC-2 on Erk Signaling
NCI-H23

	DMSO	0.1 μM LC-2	0.25 μM LC-2	1.0 μM LC-2	2.5 μM LC-2	10 μM LC-2	100 nM MRTX849	10 μM LC-1
KRAS	N/A	N.S.	*	****	*****	N.S.	N.S.	N.S.
pErk	N/A	N.S.	N.S.	N.S.	*	N.S.	*	*

Supporting Information Table 2: Two-way ANOVA analysis of Figure 5B. Not Significant (N.S.); * $p < 0.05$; **** $p < 0.001$.

Effects of LC-2 on Erk Signaling
at 6 and 24 hours
MIA PaCa-2

	Time (hrs)					
	6			24		
	DMSO	100 nM MRTX849	2.5 μM LC-2	DMSO	100 nM MRTX849	2.5 μM LC-2
KRAS	N/A	N.S	**	N.S	N.S	**
pErk	N/A	****	**	N.S	*	**

Supporting Information Table 3: Two-way ANOVA analysis of Figure 6A. Not Significant (N.S.); * $p < 0.05$; ** $p < 0.01$; **** $p < 0.001$.

Effects of LC-2 on KRAS Signaling at 6 and 24 hours NCI-H23

	Time (hrs)					
	6			24		
	DMSO	100 nM MRTX849	2.5 µM LC-2	DMSO	100 nM MRTX849	2.5 µM LC-2
KRAS	N/A	N.S	**	N.S	****	****
pErk	N/A	****	****	*	****	****

Supporting Information Table 4: Two-way ANOVA analysis of Figure 6B. Not Significant (N.S.); * $p < 0.05$; ** $p < 0.01$; **** $p < 0.001$.

Effect of LC-2 on KRAS Signaling 24 hour Time Course SW1573 cells

	Time (hrs)											
	1		2		4		8		12		24	
	DMSO	2.5 µM LC-2	DMSO	2.5 µM LC-2	DMSO	2.5 µM LC-2	DMSO	2.5 µM LC-2	DMSO	2.5 µM LC-2	DMSO	2.5 µM LC-2
KRAS	N/A	N.S.	N.S.	N.S.	N.S.	N.S	N.S.	**	N.S.	**	N.S.	***
pErk	N/A	****	N.S.	****	N.S.	****	*	**	****	*	****	N.S

Supporting Information Table 5: Two-way ANOVA analysis of SI Figure 4. Not Significant (N.S.); * $p < 0.05$; ** $p < 0.01$; *** $p < 0.005$; $p < 0.001$.

Materials and Methods:

Cell Lines and Reagents:

NCI-H2030 (CRL-5914), MIA PaCa-2 (CRL-1420), NCI-H23 (CRL-5800), NCI-H358 (CRL-5807), and HCT-116 (CCL-247) cells were obtained from ATCC, expanded immediately, and frozen down. Vials were thawed and used within 20 passages. SW1573 cells were a gift from Arvinas and were handled in the same manner. NCI-H2030, NCI-H23, and NCI-H358 were cultured in RPMI (ATCC 30-2001) supplemented with 10% FBS (Biological Industries; cat. no. S1480) and 1% Penicillin-Streptomycin (ThermoFisher; cat. no. 15140122). HCT-116 cells were maintained in high glucose DMEM (ThermoFisher; cat. no. 11965084) supplemented as above. MIA PaCa-2 cells were cultured in high glucose DMEM supplemented with 10% FBS, 2.5% horse serum (ThermoFisher; cat. no. 26050-088; lot 2109875), and 1% Penicillin-Streptomycin. SW1573 cells were maintained in DMEM/F12 Nutrient Mix with GlutaMAX supplement (ThermoFisher; cat. no. 10565018) with 10% FBS and 1% Penicillin-Streptomycin added. DPBS (ThermoFisher; cat. no. 14190250) was used to wash cells and 0.25% Trypsin-EDTA (ThermoFisher; cat. no. 252000-056) was used to detach cells for passaging. MRTX849 was purchased from ChemieTek (cat. no. CT-MRTX849), epoxomicin was purchased from Astatech (cat. no. 41576), MLN4924 (pevonedistat) was purchased from Selleckchem (cat. no. S7109), and bafilomycin A1 was purchased from Millipore Sigma (cat. no. B1793). The VHL ligand was generously provided by Arvinas.

Time Course Assays:

Between 2.5 x 10^5 and 6.0 x 10^5 cells were seeded into 6-well plates (Corning; cat. no. 353046). The next day, media was removed and cells were treated with 2.5 μM LC-2 for 1, 2, 4, 8, 12, or 24 hours. Cells were treated with 100 nM MRTX849 and 2.5 μM LC-2 for 6, 24, 48, or 72 hours for longer time course experiments. For 24-hour time course experiments, cells were treated at the indicated times and concurrently lysed in RIPA buffer supplemented as described previously. For longer time course experiments and time courses in which cells were treated with LC-2 or LC-2 Epimer, cells were concurrently treated with either compound, then lysed by scraping in RIPA buffer at the indicated time points.

Competition, Proteasome Inhibition, and Neddylation Inhibition Experiments

Between 2.5 x 10^5 and 5.0 x 10^5 cells were seeded into 6-well plates. The next day cells were pretreated with DMSO, 500 μM or 1 mM VHL ligand, 1 μM epoxomicin, 1 μM MLN4924, or 100 nM M bafilomycin A1 for 1 hour. Media was then removed and cells were treated with DMSO, 2.5 μM LC-2 plus DMSO, 2.5 μM LC-2 Epimer plus DMSO, or co-treated with 2.5 μM LC-2 and the corresponding competitor/inhibitor. H2030 cells were treated for 4 hours and H23 cells were treated for 24 hours, after which cells were lysed by scraping in RIPA buffer supplemented as described previously.

Immunoblotting:

Cell lysates were clarified at 21000 x g for 15 mins at 4° C. Protein levels were quantified using a 50:1 mixture of bicinchoninic acid solution (Millipore Sigma; cat. no. B9643) and 4% (w/v) copper(II) sulfate solution (Millipore Sigma; cat. no. C2284) incubated at 37° C for 30 mins. Absorbance values at 560 nm were read on an EnVision 2101 Multilabel Reader (PerkinElmer). Proteins were separated using 26 well Criterion TGX precast 4-15% (cat. no. 5671085) or 8-16% (cat. no. 5671105) gradient midi gels. After separation, proteins were transferred to nitrocellulose or PVDF membranes at 76 V for 2 hours at 4° C. Blots were then blocked in 5% milk in tris-buffered saline with Tween-20 (TBST; 20 mM Tris, 150 mM NaCl, 0.02 % Tween-20). After blocking, blots were incubated in primary antibody overnight (12-18 hours) at 4° C or for 2 hours at room temperature with mild agitation at the manufacturer's indicated dilution in either 5% milk or 5% BSA in TBST. Blots were then washed thrice with TBST for 5 mins at room temperature. After washing, blots were incubated with 1:5,000-1:10,000 of donkey anti-rabbit (GE Life Sciences; NA934) or sheep anti-mouse (GE Life Sciences; NA931) secondary antibody diluted in 5% milk for 1 hour at room temperature with mild agitation. Blots were again washed thrice with TBST for 5 mins. Chemiluminescent signal was generated using Amersham ECL Prime Western Blotting Detection Reagant (GE Life Sciences; cat. no. RPN2232) or SuperSignal West Femto Maximum Sensitivity Substrate (ThermoFisher; cat. no. 34095). Images were obtained using a Bio-Rad ChemiDoc Imager. Fluorescent α-tubulin images were collected with the Bio-Rad ChemiDoc Imager using an Alexa488 filter. The primary antibodies used in this work

include: KRAS (LSBio; clone 2C1; cat. no. LS-C175665), p-p42/44 MAPK (phospho T202/Y204) (pErk; Cell Signaling Technologies (CST); cat. no. 4370S or 9106S), p42/44 MAPK (Erk1/2; CST; cat. no. 4695S), alpha-tubulin (CST; 2144S), and alpha-tubulin w/ AlexaFluor488 (Millipore; cat. no. 16-232).

Quantification and Statistical Analysis:

Band intensities were quantified using BioRad's Image Lab Software. Total KRAS levels were examined by quantifying levels of both conjugated $KRAS^{G12C}$ and unbound KRAS (wt or mutant) using an analysis box that spanned the two bands. This same sized box was used to quantify unbound KRAS in DMSO treated samples to account for background, except for LC-2 Epimer in Figure 3. To quantify LC-2 Epimer engagement only the top, PROTAC bound, band was quantified and band intensity was normalized to unbound KRAS in DMSO treated samples using a similar sized analysis box. Data was analyzed by computing one-way ANOVAs or two-way ANOVAs (for grouped data) using multiple comparisons in which the mean of DMSO was compared to all treatment means using GraphPad Prism 7. For time courses, protein levels were compared to DMSO for each time point. DC_{50} and D_{Max} were quantified by fitting data to an inhibitor vs. dose response non-linear regression using GraphPad Prism 7.

Chemical synthesis

A. General considerations. Chemicals used for synthesis were purchased from commercial sources and were used without further purification. Flash chromatography was performed using Biotage flash chromatography system using pre-packed columns. ^{1}H NMR and ^{13}C NMR spectra were recorded on an Agilent DD2 600 NMR spectrometer (600 MHz for ^{1}H and 151 MHz for ^{13}C). The values of chemical shifts (δ) are reported in p.p.m. Coupling constants (*J*) are reported in Hz. High-resolution mass spectra (HRMS) were recorded on a Waters Xevo QTOF LCMS with ESI using a Waters Acquity UPLC. HPLC purifications were performed on a reverse-phase column using a Gilson HPLC system.

B. Experimental protocols.

Synthesis of **3**:

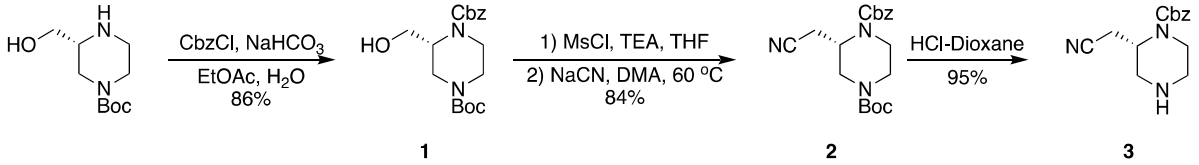

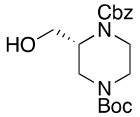

1-benzyl 4-(*tert*-butyl) (*R*)-2-(hydroxymethyl)piperazine-1,4-dicarboxylate (**1**)

To a solution of tert-butyl (3R)-3-(hydroxymethyl)piperazine-1 -carboxylate (5.0 g, 1.0 eq) in Ethyl acetate (100 mL) was added $NaHCO_3$ (3.0 eq), H_2O (50 mL) and benzyl carbonochloridate (1.30 eq). The mixture was stirred at 25 °C. for 12 hour. After completion, the organic phase was separated, washed with water (100 mLX2) dried over Na_2SO_4 and filtered. The solvent was removed under vacuum to give the title compound (7.0 g, 86% yield) as a yellow oil, which was used in the next step without further purification.

LCMS [ESI, M+1]: 351.

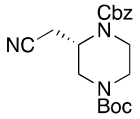

1-benzyl 4-(*tert*-butyl) (*S*)-2-(cyanomethyl)piperazine-1,4-dicarboxylate (**2**)

To a solution of I-benzyl 4-tert-butyl (2R)-2-(hydroxymethyl) piperazine-l,4-dicarboxylate (7.0 g, 1.0 eq) in THF (100 mL) was added TEA (3.0 eq) and methanesulfonyl chloride (1.2 eq). The mixture was stirred at 20 °C. for one hour. The reaction mixture was quenched by addition H2O 50 mL at 20 °C. The reaction mixture was extracted with ethyl acetate (100 mLx2). The organic layers were washed with H_2O (100 mL), dried over Na_2SO_4, and filtered. The solvent was removed under vacuum. 1-benzyl 4-tert-butyl (2R)-2-(methylsulfonyloxymethyl) piperazine-l,4-dicarboxylate was obtained as a yellow oil. The crude product was used directly to the next step without further purification.

To a solution of 1-benzyl 4-tert-butyl (2R)-2-(methylsulfonyloxymethyl)piperazine-1,4-dicarboxylate in DMA (150 mL) was added NaCN (4 eq.). The mixture was stirred at 60 °C. for 12 hour. The solvent was removed under vacuum to give an oil residue. The residue was diluted with H_2O (40 mL) and extracted with ethyl acetate (50 mLx3). The combined organic layers were washed with saturated brine, dried over Na_2SO_4, filtered and concentrated under reduced

pressure to give a residue. The residue was purified by column chromatography (SiO_2, Hexanes/Ethyl acetate=5:1 to 3:1) to give the title compound (6.0 g, two steps yield 84 %) as a yellow oil.

^{1}H NMR (600 MHz, $CDCl_3$) δ 7.40-7.32 (m, 5H), 5.16 (s, 2H), 4.55 (s, 1H), 4.25-3.80 (m, 3H), 2.95-3.25 (m, 2H), 2.85 (s, 1H), 2.60 (d, *J* = 50.2 Hz, 1H), 2.74-2.40 (m, 2H).

^{13}C NMR (150 MHz, $CDCl_3$) δ 154.9, 154.6, 135.8, 128.6, 128.4, 128.2, 116.7, 81.0, 68.0, 48.2, 45.3, 42.4, 39.2, 28.3, 19.1.

HRMS [$C_{19}H_{25}N_3O_4Na^+$] Cal: 382.1737; Obs: 382.1743.

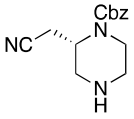

benzyl (*S*)-2-(cyanomethyl)piperazine-1-carboxylate (**3**)

To a solution of I-benzyl 4-tert-butyl (2S)-2-(cyanomethyl) piperazine-l,4-dicarboxylate (6.0 g, 1.0 eq) in dioxane (20.8 mL) was added 4.0 M HCl in dioxane (20.8 mL, 5.0 eq). The mixture was stirred at 20 °C. for 1 hour. Then $NaHCO_3$ was added to the reaction mixture until a pH>7 was reached, after which the reaction was concentrated under reduced pressure to remove dioxane. The residue was diluted with H_2O (50 mL) and extracted with ethyl acetate (50 mLx3). The combined organic layers were washed with H_2O (20 mL), dried over Na_2SO_4, filtered and concentrated under reduced pressure to give a residue. The product benzyl (2S)-2-(cyanomethyl) piperazine-1-carboxylate (4.1 g, 95% yield) was obtained as a yellow oil.

Synthesis of **15**:

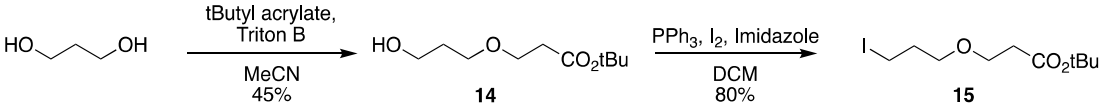

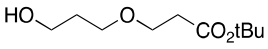

tert-butyl 3-(3-hydroxypropoxy)propanoate (**14**)

To a solution of propane 1,3-diol (20 mmol, 1.5 g, 1.0 eq.) in acetonitrile (20 mL) was added Triton B (0.3 eq.), and tert-butyl 3-(3-hydroxypropoxy)propanoate (1.0 eq.). The mixture was stirred at 20 °C overnight and concentrated under vacuum. The residue was purified by column chromatography (SiO_2, Hexanes/Ethyl acetate=5:1 to 1:1) to give the title compound as a colorless oil (1.85 g, 45% yield).

^{1}H NMR (600 MHz, $CDCl_3$) δ 3.77 – 3.72 (m, 2H), 3.67 (t, *J* = 6.2 Hz, 2H), 3.65 – 3.60 (m, 2H), 2.48 (t, *J* = 6.2 Hz, 2H), 1.83 – 1.78 (m, 2H), 1.44 (s, 9H).

^{13}C NMR (150 MHz, $CDCl_3$) δ 171.1, 80.8, 70.1, 66.7, 61.8, 36.2, 31.9, 28.0.

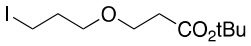

tert-butyl 3-(3-iodopropoxy)propanoate (**15**)

14 (1.85 g, 1.0 eq.) was dissolved in dichloromethane (30 mL) and triphenylphosphine (1.1 eq.) was added followed by imidazole (1.2 eq.). I_2 (1.1 eq.) was added portion wise and the reaction mixture was stirred overnight at 20 °C. The reaction mixture was quenched with a saturated aqueous solution of sodium thiosulfate and stirred for 20 minutes. The organic layer was separated and the aqueous extracted with dichloromethane. The organic layers were combined, washed with brine, dried over Na_2SO_4 and concentrated *in vacuo*. The residue was purified by column chromatography (SiO_2, Hexanes/Ethyl acetate=0:1 to 3:1) to yield the title compound (2.01 g, 80% yield).

^{1}H NMR (600 MHz, $CDCl_3$) δ 3.66 (t, *J* = 6.4 Hz, 2H), 3.48 (t, *J* = 5.8 Hz, 2H), 3.25 (t, *J* = 6.8 Hz, 2H), 2.46 (t, *J* = 6.4 Hz, 2H), 2.03 (tt, *J* = 6.9, 5.8 Hz, 2H), 1.44 (s, 9H).

^{13}C NMR (150 MHz, $CDCl_3$) δ 170.8, 80.5, 70.1, 66.5, 36.3, 33.3, 28.1, 3.3.

HRMS [$C_{10}H_{19}INaO_3^+$] Cal: 337.0271; Obs: 337.2077.

Synthesis of **6**:

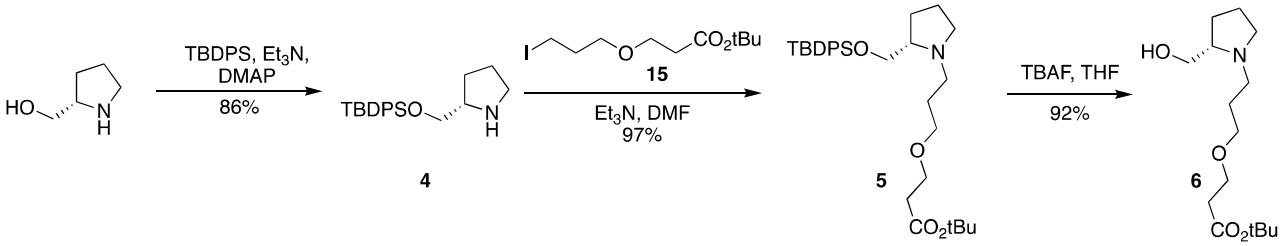

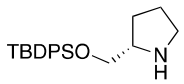

(*S*)-2-(((*tert*-butyldiphenylsilyl)oxy)methyl)pyrrolidine (**4**)

To a solution of (S)-(+)-2-Pyrrolidinemethanol (1.0 g, 1.0 eq.) in THF was added tert-butyl-chloro-diphenyl-silane (1.2 eq.), DMAP (0.1 eq.), and TEA (3.0 eq.). The mixture was stirred at 20 °C overnight and concentrated under vacuum. The residue was purified by column chromatography (SiO_2, DCM/Methanol=1:0 to 10:1) to give the title compound as a yellow oil (2.9 g, 86% yield).

^{1}H NMR (600 MHz, $CDCl_3$) δ 7.68 – 7.65 (m, 4H), 7.44-7.35 (m, 6H), 3.68 (dd, *J* = 10.3, 4.8 Hz, 1H), 3.61 (dd, *J* = 10.1, 6.1 Hz, 1H), 3.32-3.26 (m, 1H), 3.04-2.98 (m, 1H), 2.93-2.87 (m, 1H), 1.84-1.70 (m, 3H), 1.55-1.47 (m, 1H), 1.06 (s, 9H).

^{13}C NMR (150 MHz, $CDCl_3$) δ 135.6, 133.5, 133.4, 129.6, 127.7, 66.0, 59.9, 46.3, 27.4, 26.9, 25.16, 19.3.

HRMS [$C_{21}H_{30}NOSi^{+}$] Cal: 340.2091; Obs: 340.2088.

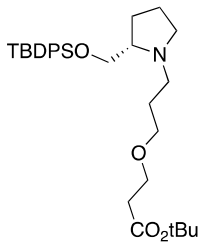

tert-butyl (*S*)-3-(3-(2-(((*tert*-butyldiphenylsilyl)oxy)methyl)pyrrolidin-1-yl)propoxy)propanoate (**5**)

To a solution of **4** (2.0 g, 1.0 eq.) in DMF was added *tert*-butyl 3-(3-iodopropoxy)propanoate (1.0 eq.) and TEA (3.0 eq.). The mixture was stirred at 20 °C overnight and concentrated under vacuum. The residue was purified by column chromatography (SiO_2, DCM/Methanol=1:0 to 10:1) to give the title compound as a yellow oil (3.0 g, 97% yield).

^{1}H NMR (600 MHz, $CDCl_3$) δ 7.80-7.56 (m, 4H), 7.51-7.37 (m, 6H), 4.56 – 3.79 (m, 4H), 3.66 – 3.44 (m, 5H), 3.36 (s, 1H), 3.06 (s, 1H), 2.53-2.31 (m, 3H), 2.26-1.99 (m, 5H), 1.90-1.78 (m, 1H), 1.60 (s, 2H), 1.43 (s, 9H), 1.08 (s, 9H).

^{13}C NMR (150 MHz, $CDCl_3$) δ 171.1, 135.7, 135.5, 130.2, 128.1, 128.0, 80.8, 70.5, 68.2, 66.4, 62.7, 54.9, 35.9, 28.1, 26.9, 25.5, 22.07, 19.1.

HRMS [$C_{31}H_{48}NO_4Si^{+}$] Cal: 526.3347; Obs: 526.3353.

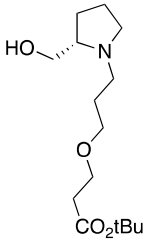

tert-butyl (*S*)-3-(3-(2-(hydroxymethyl)pyrrolidin-1-yl)propoxy)propanoate (**6**)

To a solution of **5** (3.0 g, 1.0 eq.) in THF was added TBAF (1.0 M in THF, 2.0 eq.). The mixture was stirred at 20 °C overnight and concentrated under vacuum. The residue was purified by column chromatography (SiO_2, DCM/Methanol=1:0 to 5:1) to give the title compound as a yellow oil (1.5 g, 92% yield).

HRMS [$C_{15}H_{30}NO_4^+$] Cal: 288.2169; Obs: 288.2175.

Synthesis of **LC-2**[S1]:

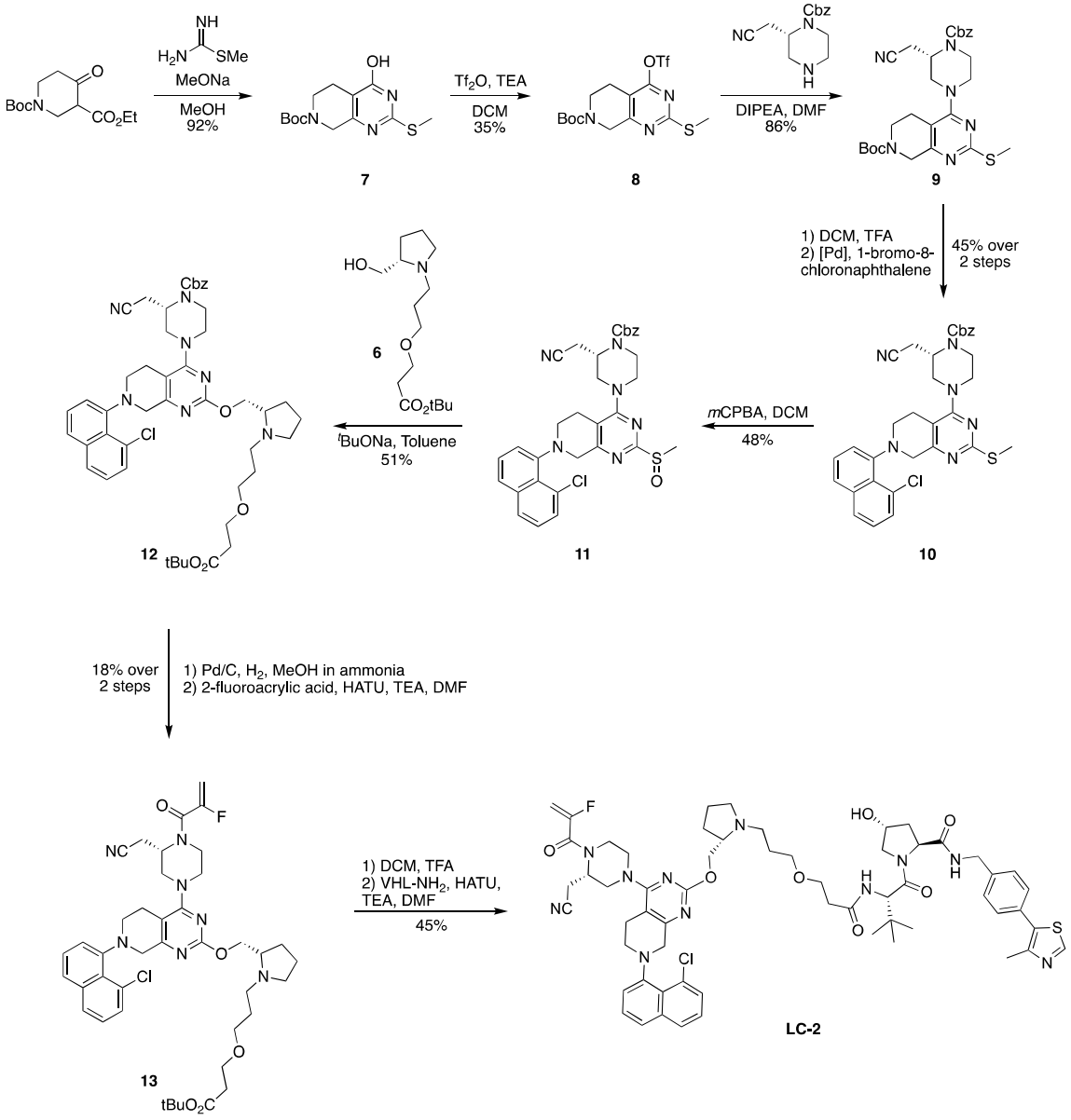

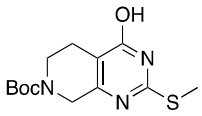

tert-butyl 4-hydroxy-2-(methylthio)-5,8-dihydropyrido[3,4-*d*]pyrimidine-7(6*H*)-carboxylate (**7**)

Step 1: To a stirred solution of 1-tert-butyl 4-ethyl 3-oxopiperidine-1,4-dicarboxylate (17.0 g, 1.0 eq) in MeOH (300 mL) at 20 °C under nitrogen was added NaOMe (5.0 eq), followed by 2-methylisothiourea (1.80 eq.) as a solid. The reaction mixture was stirred at 20 °C for 16 hours. The reaction mixture was acidified with HCl (2 M) until pH~5, and then the mixture was concentrated under reduced pressure to removed MeOH. The residue was resuspended in 300 mL of ethyl acetate and 300 mL of water and stirred rapidly. The suspension was filtered and the white solid was collected. The filtrate was separated and the organics washed with water (1x300 mL) and brine (1x200 mL). The organics were isolated, dried over Na_2SO_4, filtered and concentrated to a white solid, tert-butyl 4-hydroxy-2-methylsulfanyl-6,8-dihydro-5H-pyrido[3,4-d]pyrimidine-7-carboxylate (17.2 g, 92% yield) was obtained as a white solid and used directly for next step without further purification.

LCMS [M+1]: 298.

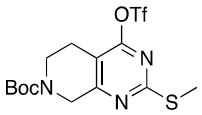

tert-butyl 2-(methylthio)-4-(((trifluoromethyl)sulfonyl)oxy)-5,8-dihydropyrido[3,4-*d*]pyrimidine-7(6*H*)-carboxylate (**8**)

Step 2: To a stirred suspension of **7** (10 g, 1.0 eq) in DCM (200 mL) at 0 °C was added DIEA (2.0 eq.) followed by Tf_2O (1.5 eq.) under nitrogen. Immediately a brown solution formed. After stirring at 25 °C for 16 hours, the reaction was concentrated to give a brown oil. The brown oil was purified by column chromatography (SiO2, Hexanes/Ethyl acetate=1/0 to 10/1) to give the title compound (5.1 g, 35% yield) as a yellow solid.

HRMS [$C_{14}H_{19}F_3N_3O_5S_2$+] Cal: 430.0713; Obs: 430.0718.

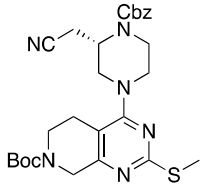

tert-butyl (*S*)-4-(4-((benzyloxy)carbonyl)-3-(cyanomethyl)piperazin-1-yl)-2-(methylthio)-5,8-dihydropyrido[3,4-*d*]pyrimidine-7(6*H*)-carboxylate (**9**)

Step 3: A mixture of **8** (1.24 g, 1.0 eq), benzyl-(2S)-2-(cyanomethyl)piperazine-1-carboxylate (1.05 eq), and DIEA (3.0 eq) in DMF (10 mL) was degassed and purged with N_2 3 times, and then the mixture was stirred at 100 °C for 1 hour under N_2 atmosphere. After completion, the solvent was removed under vacuum. The residue was purified by column chromatography (SiO_2, Hexanes/ Ethyl acetate=3/1 to 1:1) to give title compound (1.36 g, 86% yield) as a yellow solid.

^{1}H NMR (600 MHz, $CDCl_3$) δ 7.43 – 7.30 (m, 5H), 5.17 (s, 2H), 4.72 – 4.55 (m, 2H), 4.36 (d, *J* = 19.1 Hz, 1H), 4.02 – 3.71 (m, 3H), 3.40 – 3.21 (m, 4H), 2.98 (t, *J* = 12.2 Hz, 1H), 2.75 – 2.57 (m, 4H), 2.49 (s, 3H), 1.47 (s, 9H).

^{13}C NMR (151 MHz, $CDCl_3$) δ 168.61, 164.66, 135.82, 128.68, 128.65, 128.45, 128.29, 128.26, 128.23, 117.00, 111.12, 68.07, 60.39, 48.50, 47.84, 28.41, 28.02, 25.88, 21.05, 19.16, 17.59, 14.19, 14.05.

HRMS [$C_{27}H_{35}N_6O_4S^+$] Cal: 539.2435; Obs: 539.2438.

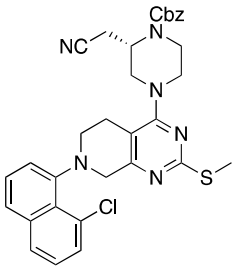

benzyl (*S*)-4-(7-(8-chloronaphthalen-1-yl)-2-(methylthio)-5,6,7,8-tetrahydropyrido[3,4-*d*]pyrimidin-4-yl)-2-(cyanomethyl)piperazine-1-carboxylate (**10**)

Step 4: A mixture of **9** (1.36 g , 1.0 eq), TFA (6.8 mL) in DCM (6.8 mL) was degassed and purged with N_2 3 times, and then the mixture was stirred at 20°C for 1 hour under N_2 atmosphere. After completion, the reaction mixture was quenched with saturated $NaHCO_3$ solution. The mixture was extracted with ethyl acetate (3x50 mL) and the organic layer was dried over Na_2SO_4 and filtered. The solvent was removed under vacuum to give benzyl (*S*)-2-(cyanomethyl)-4-(2-(methylthio)-5,6,7,8-tetrahydropyrido[3,4-*d*]pyrimidin-4-yl)piperazine-1-carboxylate (1.11 g, crude) as a yellow solid which was used for the next step without further purification.

Step 5: A mixture of benzyl (2S)-2-(cyanomethyl)-4-(2-methylsulfanyl-5,6,7,8-tetrahydropyrido[3,4-d]pyrimidin-4-yl)piperazine-l-carboxylate (1.11 g, 1.0 eq.), 1-bromo-8-chloro-naphthalene (1.8 eq.), $Pd_2(dba)_3$ (0.1 eq.), RuPhos (0.2 eq.) and Cs2CO3 (3.6 eq.) in

toluene (10 mL) was degassed and purged with N_2 3 times, and then the mixture was stirred at 100 °C for 12 hours under N_2 atmosphere. After completion, the reaction mixture was filtered. The organic solvent was removed under vacuum to give an oil residue. The residue was purified by column chromatography (SiO_2, Hexanes/Ethyl acetate=5:1 to 3:1) to give the title compound (0.77 g, two steps yield 45%) as a dark yellow solid.

HRMS [$C_{32}H_{32}ClN_6O_2S^+$] Cal: 599.1990; Obs: 599.1996.

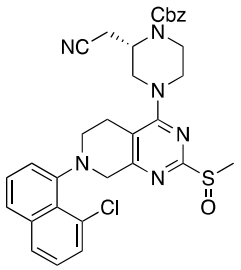

benzyl (2*S*)-4-(7-(8-chloronaphthalen-1-yl)-2-(methylsulfinyl)-5,6,7,8-tetrahydropyrido[3,4-*d*]pyrimidin-4-yl)-2-(cyanomethyl)piperazine-1-carboxylate (**11**)

Step 6: A mixture of **10** (734 mg, 1.0 eq), m-CPBA (0.6 eq.) in DCM (8 mL) was stirred at 0 °C for 30 min. After which another batch of m-CPBA (0.6 eq.) was added and the mixture was stirred for another 30 min at 0 °C. After completion, the reaction was quenched with water (10 mL). The mixture was extracted with ethyl acetate (3x10 mL). The combined organic layer was dried with Na_2SO_4 and filtered. The solvent was removed to give an oil residue. The residue was purified by column chromatography (SiO_2, Methanol/Ethyl acetate=0:1 to 1:10) to give the title compound (350 mg, 46% yield) as a yellow solid.

LC-MS [ESI, M+1] = 616.

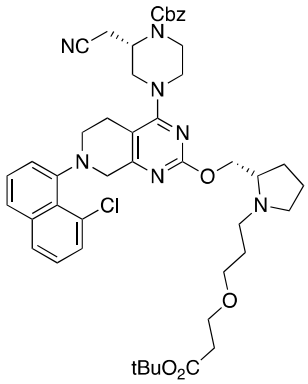

benzyl (*S*)-4-(2-(((*S*)-1-(3-(3-(*tert*-butoxy)-3-oxopropoxy)propyl)pyrrolidin-2-yl)methoxy)-7-(8-chloronaphthalen-1-yl)-5,6,7,8-tetrahydropyrido[3,4-*d*]pyrimidin-4-yl)-2-(cyanomethyl)piperazine-1-carboxylate (**12**)

Step 7: To a solution of **11** (350 mg, 1.0 eq.) and *tert*-butyl (*S*)-3-(3-(2-(hydroxymethyl)pyrrolidin-1-yl)propoxy)propanoate (**6**) (3.0 eq.) in toluene (5 mL) was added *t*-BuONa (3.0 eq.). The mixture was stirred at 0 °C. for 0.5 hour. After completion, the mixture was added to cold water (5 mL) and extracted with ethyl acetate (3x5 mL). The combined organic layer was dried over Na_2SO_4, filtered and concentrated. The obtained product was purified by column chromatography (SiO_2, Ethyl acetate:Methanol=1:0 to 10:1) to give the title compound (230 mg, 44% yield) as a yellow solid.

LC-MS [ESI, M+1] = 838.

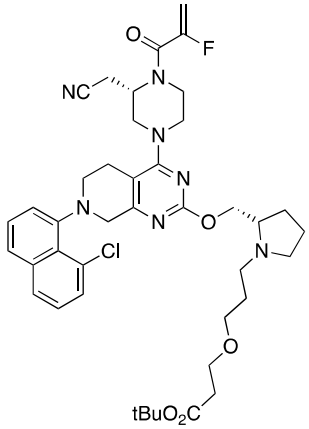

tert-butyl 3-(3-((*S*)-2-(((7-(8-chloronaphthalen-1-yl)-4-((*S*)-3-(cyanomethyl)-4-(2-fluoroacryloyl)piperazin-1-yl)-5,6,7,8-tetrahydropyrido[3,4-*d*]pyrimidin-2-yl)oxy)methyl)pyrrolidin-1-yl)propoxy)propanoate (**13**)

Step 8: To a solution of **12** (230 mg, 1.0 eq.) in MeOH (3 mL) was added 7N NH_3 in MeOH (3 mL), and Pd/C (100 mg, 10% purity) under N_2. The suspension was degassed under vacuum and purged with H_2 several times. The mixture was stirred under H_2 (15 psi) at 20 °C for 4 hours. After which another batch of Pd/C (100 mg, 10% purity) was added. The mixture was stirred under H_2 overnight. Upon completion, the catalyst was filtered off and the filtrate was concentrated under vacuum to give the title compound (100 mg, 52% yield) as a yellow solid which was used directly in the next step without further purification. LC-MS [ESI, M+1] = 704.

Step 9: To a solution of above product (141 mg, 1.0 eq.) in DMF was added sodium 2-fluoroprop-2-enoyloxy (2.0 eq.), HATU (1.5 eq.), and TEA (4.0 eq.). The mixture was stirred at room temperature for 1 hour. After completion, the residue was diluted with H_2O (15 mL),

extracted with EtOAc (3X15 mL), dried over Na_2SO_4, concentrated under vacuum and purified by Prep-TLC (DCM:Methanol:Ammonia = 200:10:1). The title compound (42 mg, 27% yield) was obtained as a colorless oil.

LC-MS [ESI, M+1] = 776.

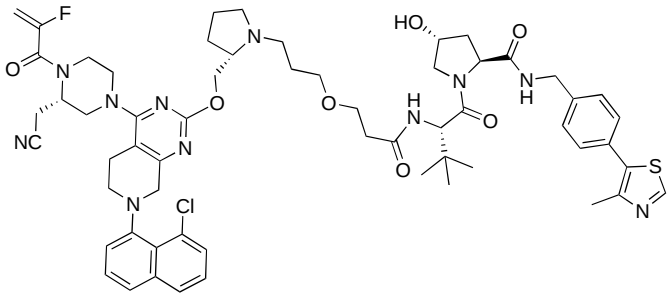

(2*S*,4*R*)-1-((*S*)-2-(3-(3-((*S*)-2-(((7-(8-chloronaphthalen-1-yl)-4-((*S*)-3-(cyanomethyl)-4-(2-fluoroacryloyl)piperazin-1-yl)-5,6,7,8-tetrahydropyrido[3,4-*d*]pyrimidin-2-yl)oxy)methyl)pyrrolidin-1-yl)propoxy)propanamido)-3,3-dimethylbutanoyl)-4-hydroxy-*N*-(4-(4-methylthiazol-5-yl)benzyl)pyrrolidine-2-carboxamide (**LC-2**)

Step 10: To a solution of **13** (21 mg, 1.0 eq.) in DCM (1 mL) was added TFA (1 mL). The mixture was stirred for 0.5 hour at room temperature, concentrated under vacuum and used in the next step without further purification.

To a solution of above product (1.0 eq.) in DMF (1 mL) was added (1R)-1-[(2S,4R)-4-hydroxy-2-[[4-(4-methylthiazol-5-yl)phenyl]methylcarbamoyl]pyrrolidine-1-carbonyl]-2,2-dimethyl-propyl (1.2 eq.), HATU (1.3 eq.), and TEA (5.0 eq.). The mixture was stirred for 1 hour at room temperature. Upon completion, the mixture was diluted with H_2O (5 mL), extracted with EtOAc (3X5 mL), dried over Na_2SO_4, concentrated under vacuum and purified by reverse phase HPLC. The title compound (10 mg, 33% yield) was obtained as a colorless oil.

^{1}H NMR (600 MHz, Acetone-d_6) δ 8.82 (s, 1H), 7.86 (t, *J* = 7.9 Hz, 2H), 7.70 (dd, *J* = 8.0, 3.9 Hz, 1H), 7.55 (dd, *J* = 7.3, 3.6 Hz, 1H), 7.53 – 7.48 (m, 1H), 7.45 (dd, *J* = 7.8, 4.2 Hz, 2H), 7.43 – 7.39 (m, 1H), 7.39 – 7.33 (m, 3H), 7.29 – 7.24 (m, 1H), 5.33 – 5.20 (m, 2H), 4.64 (dd, *J* = 9.3, 1.6 Hz, 1H), 4.60 – 4.48 (m, 3H), 4.39 – 4.27 (m, 3H), 4.24 – 4.08 (m, 2H), 3.87 – 3.78 (m, 2H), 3.78 – 3.70 (m, 2H), 3.67 – 3.53 (m, 3H), 3.53 – 3.43 (m, 3H), 3.37 (dd, *J* = 13.8, 3.8 Hz, 1H), 3.34 – 3.24 (m, 2H), 3.25 – 3.12 (m, 4H), 3.13 – 2.96 (m, 4H), 2.81 – 2.75 (m, 1H), 2.71 – 2.65 (m, 1H), 2.48 – 2.39 (m, 4H), 2.39 – 2.32 (m, 1H), 2.26 – 2.18 (m, 1H), 2.18 – 2.11 (m, 1H), 2.11 – 2.06 (m, 1H), 1.91 – 1.82 (m, 1H), 1.79 – 1.61 (m, 6H), 0.96 (s, 9H).

^{13}C NMR (151 MHz, Acetone-d_6) δ 172.63, 171.41, 171.34, 170.96, 167.67, 166.06, 163.77, 157.79 (d, *J* = 269.1 Hz), 151.29, 149.67, 149.41, 149.18, 140.54, 138.50, 132.37, 131.35,

130.64, 130.53, 129.92, 129.43, 128.76, 127.78, 126.77, 126.71, 125.92 (d, *J* = 11.3 Hz), 119.93, 118.28, 110.17, 77.33, 70.71, 69.85, 69.83, 67.74, 63.39, 60.60, 59.97, 59.75, 57.59, 57.46, 54.95, 53.23, 51.27, 51.21, 43.20, 38.44, 38.43, 37.41, 36.50, 32.70, 26.98, 26.86, 26.41, 24.05, 23.39, 20.89, 19.43, 16.41, 14.56, 14.41.

HRMS [$C_{59}H_{72}ClFN_{11}O_7S^+$] Cal: 1132.5004; Obs: 1132.5010.

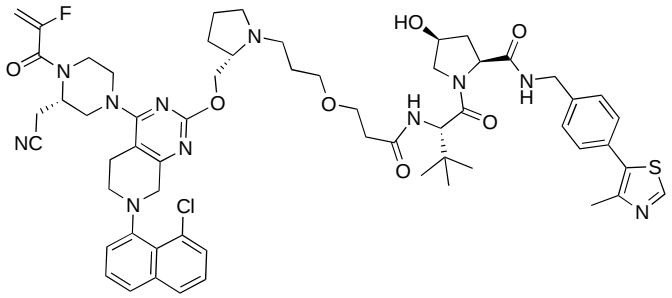

(2*S*,4*S*)-1-((*S*)-2-(3-(3-((*S*)-2-(((7-(8-chloronaphthalen-1-yl)-4-((*S*)-3-(cyanomethyl)-4-(2-fluoroacryloyl)piperazin-1-yl)-5,6,7,8-tetrahydropyrido[3,4-*d*]pyrimidin-2-yl)oxy)methyl)pyrrolidin-1-yl)propoxy)propanamido)-3,3-dimethylbutanoyl)-4-hydroxy-*N*-(4-(4-methylthiazol-5-yl)benzyl)pyrrolidine-2-carboxamide (**LC-2- Epimer**)

To a solution of **13** (21 mg, 1.0 eq.) in DCM (1 mL) was added TFA (1 mL). The mixture was stirred for 0.5 hour at room temperature, concentrated under vacuum and used in the next step without further purification.

To a solution of above product (1.0 eq.) in DMF (1 mL) was added (1R)-1-[(2S,4S)-4-hydroxy-2-[[4-(4-methylthiazol-5-yl)phenyl]methylcarbamoyl]pyrrolidine-1-carbonyl]-2,2-dimethyl-propyl (1.2 eq.), HATU (1.3 eq.), and TEA (5.0 eq.). The mixture was stirred for 1 hour at room temperature. Upon completion, the mixture was diluted with H_2O (5 mL), extracted with EtOAc (3X5 mL), dried over Na_2SO_4, concentrated under vacuum and purified by reverse phase HPLC. The title compound (4.4 mg, 15% yield) was obtained as a colorless oil.

^{1}H NMR (400 MHz, Acetone-d_6) δ 8.82 (s, 1H), 7.87 (d, *J* = 8.5 Hz, 1H), 7.70 (dd, *J* = 8.1, 2.6 Hz, 1H), 7.59 – 7.53 (m, 1H), 7.52 – 7.32 (m, 7H), 7.24 (dd, *J* = 9.4, 3.3 Hz, 1H), 5.37 – 5.17 (m, 2H), 5.00 – 4.83 (m, 1H), 4.67 – 4.57 (m, 2H), 4.51 (d, *J* = 9.6 Hz, 1H), 4.40 – 4.22 (m, 4H), 4.21 – 3.95 (m, 4H), 3.87 – 3.71 (m, 4H), 3.66 – 3.46 (m, 7H), 3.33 – 3.25 (m, 2H), 3.23 – 3.11 (m, 2H), 2.83 – 2.62 (m, 4H), 2.53 – 2.33 (m, 6H), 2.32 – 2.24 (m, 2H), 2.22 – 2.11 (m, 2H), 1.95 (d, *J* = 2.8 Hz, 1H), 1.91 (s, 2H), 1.78 – 1.62 (m, 4H), 0.97 (s, 9H).

HRMS [$C_{59}H_{72}ClFN_{11}O_7S^+$] Cal: 1132.5004; Obs: 1132.4999.

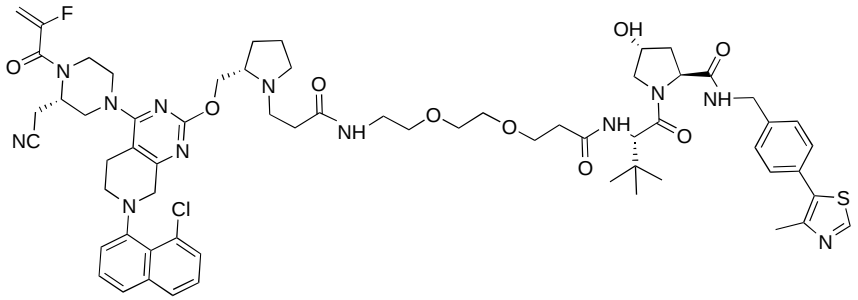

(2*S*,4*R*)-1-((*S*)-2-(*tert*-butyl)-16-((*S*)-2-(((7-(8-chloronaphthalen-1-yl)-4-((*S*)-3-(cyanomethyl)-4-(2-fluoroacryloyl)piperazin-1-yl)-5,6,7,8-tetrahydropyrido[3,4-*d*]pyrimidin-2-yl)oxy)methyl)pyrrolidin-1-yl)-4,14-dioxo-7,10-dioxa-3,13-diazahexadecanoyl)-4-hydroxy-*N*-(4-(4-methylthiazol-5-yl)benzyl)pyrrolidine-2-carboxamide (**LC-1**)

LC-1 was synthesized using the same procedure as for **LC-2** except that in step 7, *tert*-butyl (*S*)-3-(2-(hydroxymethyl)pyrrolidin-1-yl)propanoate was used instead of *tert*-butyl (*S*)-3-(3-(2-(hydroxymethyl)pyrrolidin-1-yl)propoxy)propanoate (**6**), and in step 10, (2S,4R)-1-((S)-2-amino-16,16-dimethylheptadecanoyl)-4-hydroxy-*N*-(4-(4-methylthiazol-5-yl)benzyl)pyrrolidine-2-carboxamide was used instead of (2S,4R)-1-((S)-2-(2-(2-aminoethoxy)ethoxy)acetamido)-3,3-dimethylbutanoyl)-4-hydroxy-*N*-(4-(4-methylthiazol-5-yl)benzyl)pyrrolidine-2-carboxamide.

^{1}H NMR (600 MHz, Methanol-d_4) δ 8.84 (s, 1H), 7.80 (d, *J* = 8.2 Hz, 1H), 7.65 (dd, *J* = 8.2, 2.7 Hz, 1H), 7.52 – 7.46 (m, 2H), 7.46 – 7.41 (m, 2H), 7.41 – 7.36 (m, 3H), 7.32 – 7.27 (m, 1H), 5.38 – 5.23 (m, 2H), 4.63 (s, 1H), 4.55 (t, *J* = 8.4 Hz, 1H), 4.48 (d, *J* = 11.6 Hz, 2H), 4.41 – 4.36 (m, 1H), 4.35 – 4.24 (m, 4H), 4.16 (d, *J* = 13.6 Hz, 1H), 4.11 – 4.02 (m, 2H), 3.87 (d, *J* = 10.9 Hz, 1H), 3.77 (dd, *J* = 11.0, 3.9 Hz, 1H), 3.72 – 3.52 (m, 5H), 3.46 (dt, *J* = 7.4, 5.5 Hz, 2H), 3.38 – 3.27 (m, 9H), 3.25 – 3.04 (m, 6H), 2.91 (dd, *J* = 17.1, 6.9 Hz, 1H), 2.79 – 2.58 (m, 2H), 2.54 – 2.36 (m, 8H), 2.23 – 2.16 (m, 1H), 2.10 – 2.02 (m, 2H), 1.90 – 1.71 (m, 3H), 1.40 – 1.25 (m, 3H), 0.99 (d, *J* = 1.8 Hz, 9H).

^{13}C NMR (151 MHz, Methanol-d_4) δ 174.57, 174.51, 173.14, 173.07 (d, *J* = 220.9 Hz), 167.96, 167.80, 166.82, 163.67, 152.99, 149.85 (d, *J* = 21.0 Hz), 149.19, 140.42, 139.06, 133.53, 131.67, 131.08, 131.02, 130.94, 130.51, 129.23, 126.96, 126.52, 126.49, 120.29, 111.58, 110.40, 71.20, 70.56, 69.01, 68.13, 65.89, 61.69, 61.01, 60.59, 60.44, 59.03, 58.23, 55.36, 52.77, 52.73, 51.29, 43.84, 40.51, 39.16, 37.78, 37.37, 36.98, 35.24, 33.93, 29.22, 27.64, 27.51, 27.43, 24.15, 21.01, 16.02, 14.61, 11.58.

HRMS [$C_{63}H_{79}ClFN_{12}O_{9}S$] Cal: 1233.5481; Obs: 1233.5490.

References:

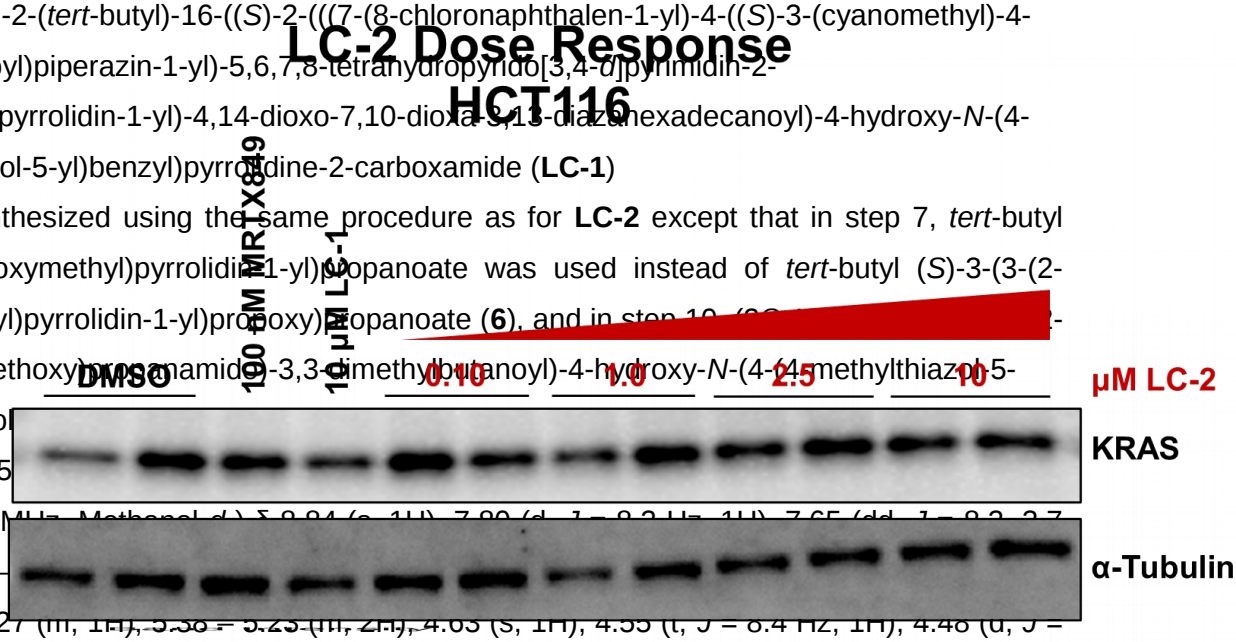

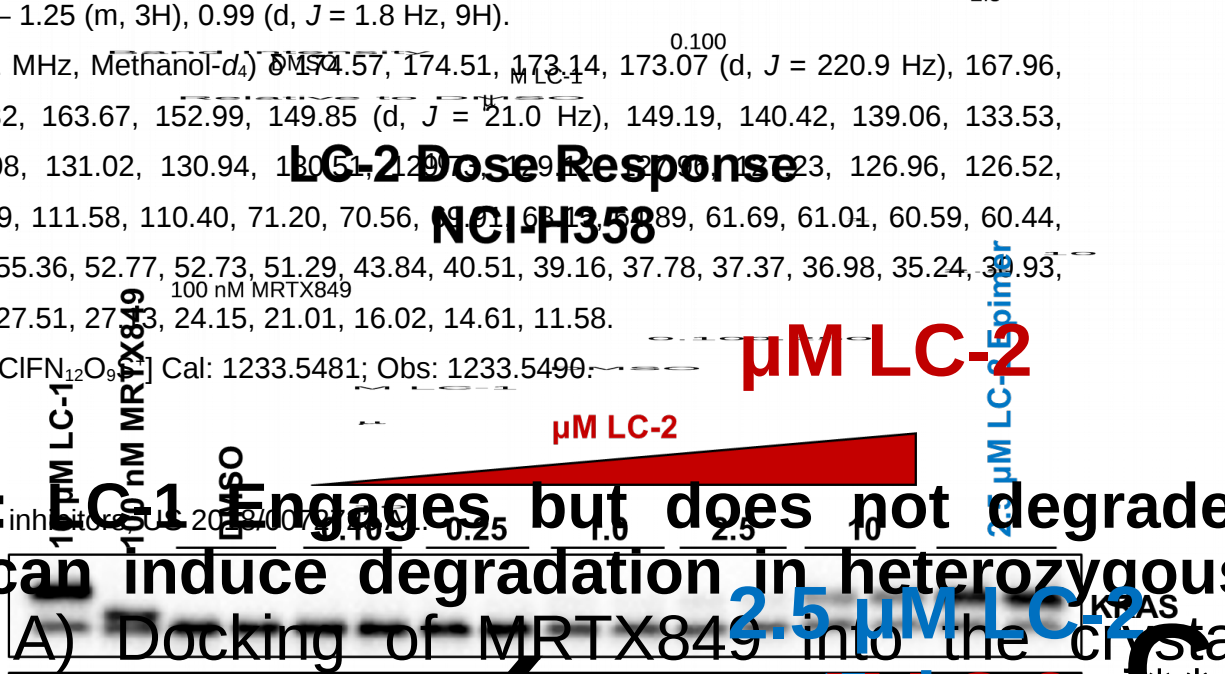

SI Figure 1: LC-1 Engages but does not degrade, while LC-2 can induce degradation in heterozygous H358 cells. A) Docking of MRTX849 into the crystal structure of KRAS G12C (PDB: 5V9U). MRTX849 is

Supporting Information.docx (2.68 MiB) view on ChemRxiv • download file